AFCRL-67-0563
OCTOBER 1967
AIR FORCE SURVEYS IN GEOPHYSICS, NO. 198

AIR FORCE CAMBRIDGE RESEARCH LABORATORIES
L. G. HANSCOM FIELD, BEDFORD, MASSACHUSETTS

Gemini V D4/D7 Spectral Measurements of Space Objects and Earth-Cloud Backgrounds

J. LOVETT
L. MARCOTTE
R. NADILE

Sponsored by
Advanced Research Projects Agency
Project VELA-UNIFORM
ARPA Order No. 363

OFFICE OF AEROSPACE RESEARCH
United States Air Force

AFCRL-67-0563
OCTOBER 1967
AIR FORCE SURVEYS IN GEOPHYSICS, NO. 198

OPTICAL PHYSICS LABORATORY PROJECT 8662

AIR FORCE CAMBRIDGE RESEARCH LABORATORIES

L. G. HANSCOM FIELD, BEDFORD, MASSACHUSETTS

Gemini V D4/D7 Spectral Measurements of Space Objects and Earth-Cloud Backgrounds

J. LOVETT
L. MARCOTTE
R. NADILE

Sponsored by
Advanced Research Projects Agency
Project VELA-UNIFORM
ARPA Order No. 363

OFFICE OF AEROSPACE RESEARCH
United States Air Force

Abstract

Results of the radiometric and interferometric optical measurements performed by the crew of Gemini V during the D4/D7 experiment are presented. With use of a rapid-scan Michelson PbS Interferometer and two radiometer channels filtered at 2.2μ and 4000 Å, measurements of earth and lunar reflected sunlight are compared to those obtained on the Gemini VII flight. Also included are detailed calibrations of the D4/D7 instrumentation used on Gemini V.

Contents

Illustrations

Tables

BLANK PAGE

Gemini V D4/D7 Spectral Measurements of Space Objects and Earth-Cloud Backgrounds

I. INTRODUCTION

The study of the spectral irradiance of natural phenomena and man-made objects has been of increasing interest in recent years, both to the scientific community and to the Department of Defense. The purpose of the Air Force D4/D7 experiment has been to obtain accurate measurements from space of emitted and reflected radiance from a comprehensive collection of subjects. The determination of threshhold sensitivity values in absolute numbers and the separation and correlation of specific targets with various backgrounds have been prime objectives.

This is a report on the most significant data obtained from the D4/D7 experiment on board Gemini V, the first of two instrumented manned flights. A cursory analysis of the data was made immediately after the flight to effect suitable modifications in the Gemini VII instrumentation. Although time did not permit any major redesign in the system, the instrumentation and operational procedures used on Gemini VII were improved as a direct result of the experience gained from the 7-day Gemini V flight. The larger amount of data received from Gemini VII was analyzed first because of the superior quality and greater availability of correlating information. The Gemini V data presented here, although less extensive, supplement and confirm the results obtained on the Gemini VII flight (Nadile, Lovett, and Marcotte, 1967b).

(Received for publication 28 September 1967)

2. INSTRUMENTATION

The D4/D7 instrumentation consisted of two interferometer spectrometers (I-14 and I-15) and one radiometer (E3G) mounted on the adapter section of the Gemini V spacecraft. All three instruments were manufactured by Block Engineering, Inc., and were boresighted to the longitudinal axis of the spacecraft (Figure 1). The instrument characteristics were a compromise to allow measurement of a comprehensive selection of targets over a broad spectral region. By necessity, the analog nature of the interferometer outputs had to be preserved, and therefore the I-14 and I-15 were provided with an onboard FM recorder which was recovered at the end of the flight. In addition, provisions were made to transmit simultaneously the interferograms to selected telemetry stations via IRIG Channel E. The E3G radiometric outputs, together with the housekeeping functions of all the instrumentation, were commutated and transmitted to ground stations within telemetry range.

Figure 1. Location of Instruments

The three-detector E3G radiometer was provided with a 10-position filter wheel controlled by the astronauts in one of three stepping modes. During initial operation in the second orbit of the flight, the filter wheel "froze" on position 8 restricting the radiometric data obtained to 4000 Å, 2.2μ, and 4.3μ (Brentnall and Lovett, 1966). The interferometers operated well although plagued by faulty operation of the onboard FM tape recorder during the early orbits. This was later attributed to excessive heating of the recorder during the launch phase of the flight. By revolution 14, recorder operation was restored and used for some of the I-14 interferometer measurements. The over-all capability of the Gemini V D4/D7 instrumentation is presented graphically in Figure 2, where a spectral plot of the minimum detectable irradiance is given for each data channel along with the instrument field of view. A complete calibration of each instrument is included in Appendices A, B, and C of this report.

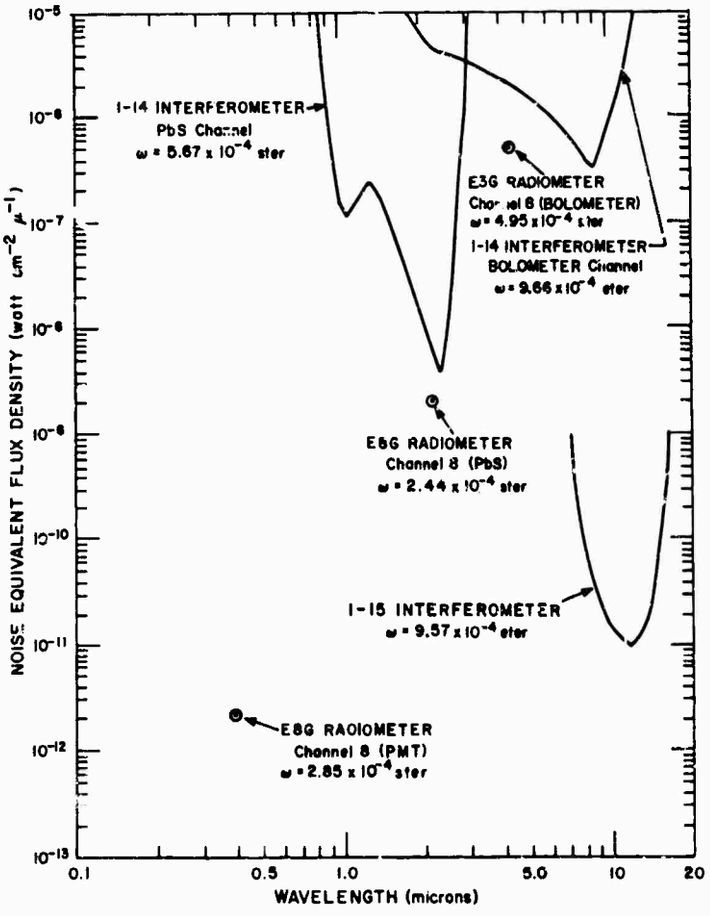

Figure 2. Noise Equivalent Flux Density of Gemini V D4/D7 Instrumentation

3. LUNAR MEASUREMENTS

Apart from the primary mission, several celestial targets were measured for three reasons: (1) To make use of the excellent opportunity afforded by a man-oriented optical system outside the earth's atmosphere; (2) to verify the optical alignment of the radiometer and interferometers with the spacecraft; and (3) to check the inflight instrument response on relatively well-known targets.

The full moon provided an almost ideal target that satisfied the foregoing requirements, and therefore an effort was made to launch both Gemini V and VII just prior to lunar opposition. A delay in the launch schedule of Gemini V made it necessary to attempt the measurement when the moon was 25 days old at a lunar phase angle of 126 degrees. This reduced the irradiance of the moon to a level below the noise of the I-14 interferometer, and thus only the 4000 Å, and 2.2-μ radiometer channels responded to the target.

Two lunar measurements were attempted during revolutions 16 and 17. The first was designed to check the instrument alignment and verify the position of maximum response for each instrument on the astronaut's sighting reticle. The second, the absolute measurement, was to be made on the following orbit, using the knowledge obtained from the previous measurement on the optical axis of the instrument to maximize the output. The peak signal attained on the alignment measurement exceeded those measured during the absolute measurement and thus a need was shown for improving the instrument boresighting mounts and the lunar alignment procedure. Suitable changes were made on Gemini VII including the procurement of photographic coverage during the moon alignment experiment to facilitate location of the field of view for each instrument. In view of the foregoing, the peak readings from the Gemini V alignment experiment were assumed to be the irradiance produced at the instrument aperture by the moon at a phase angle of 126 degrees.

It has been shown that due to the irregularities in the surface of the moon the irradiance from lunar reflected sunlight decreases more rapidly with phase angle than would be expected, assuming a relationship proportional to the illuminated area. This is shown graphically in Figure 3 (Struve, 1959) where the appropriate reduction factors for emission and reflectance are identified for a 126-deg phase angle. For purposes of comparison, the lunar irradiance as measured from Gemini VII (Condon, Lovett, Barnes, Marcotte, and Nadile, 1966) is shown in Figure 4 along with curves reduced by the foregoing phase angle factors. The only two data points obtained from Gemini V are included, and it can be seen that the 4000 Å PMT channel is in excellent agreement with the predicted curve. The PbS channel on the other hand yielded an irradiance which is a factor of 3.6 higher than the predicted value. Subsequent analysis of the earth background data obtained

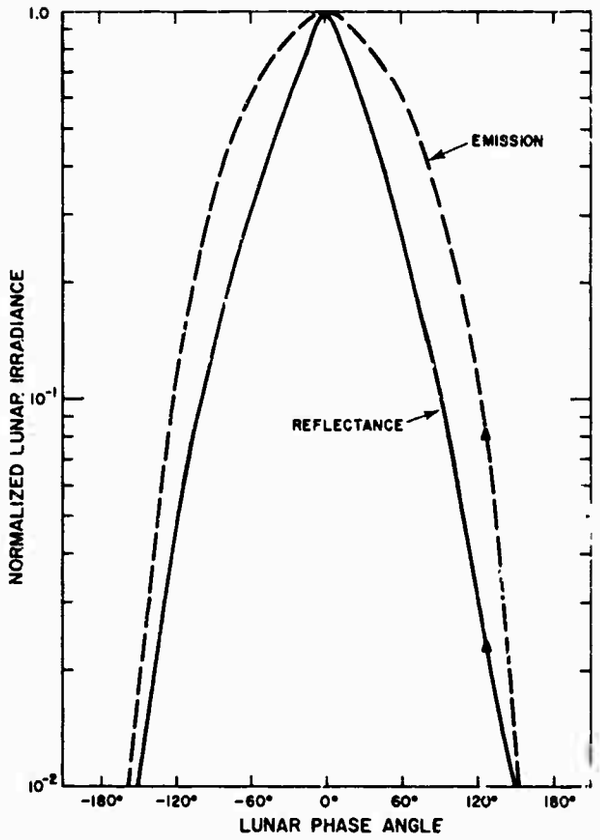

Figure 3. Lunar Irradiance as a Function of Phase Angle

later in the flight yielded radiometer values consistently higher than those of the I-14 interferometer at 2.2μ. Interestingly enough, the factor was approximately the same. Since the interferometer had the advantage of an inflight calibration lamp, the I-14 data were believed, and the decision was made to reduce all E3G lead sulphide radiometer data by the 3.6 factor, thereby bringing the 2.2μ measurement into line with the 4000 Å data and the predicted values.

The lunar self-emission is shown to illustrate its ineffectiveness at 2.2μ. A 374°K black body was assumed for the surface temperature of the illuminated surface subtending a solid angle of 5.93×10^{-5} steradians for a full moon.

4. STELLAR MEASUREMENTS

During revolutions 16 and 17, measurements of the stars Vega and Deneb were also attempted. Because of their high-color temperatures, the irradiance in the

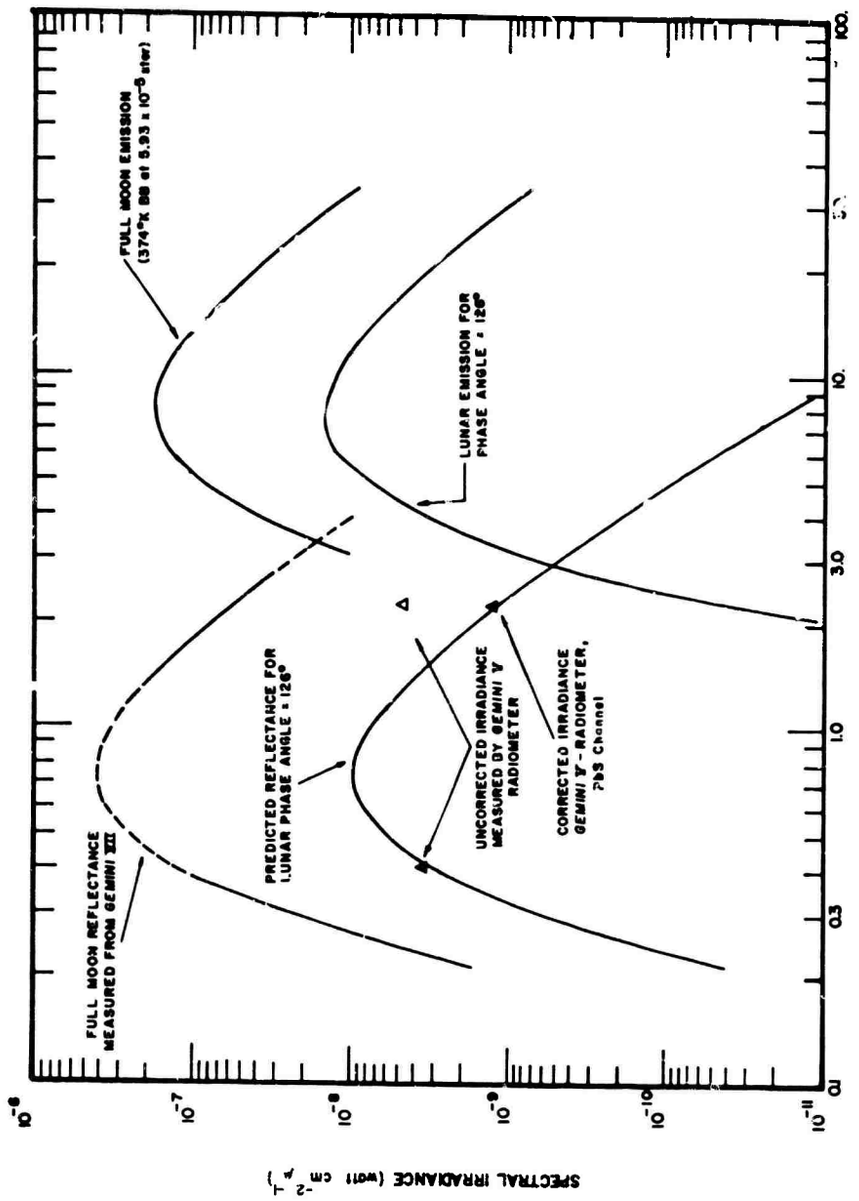

Figure 4. Moon Alignment Measurement Revolution 16

PbS region was too low to be detected. The 4000 Å PMT channel, sampling near the spectral peak of these stars, had sufficient sensitivity. The outputs obtained while boresighting on Deneb contained only 3 commutated values slightly above the noise level of the instrument. This closely resembled spurious points generated by telemetry noise and therefore was not considered to be a valid measurement. The measurement on the star Vega, however, demonstrated a continuous output reading which peaked at 1.05×10^{-11} watt $cm^{-2} \mu^{-1}$. This value is compared in Figure 5 to a predicted curve for the irradiance of Vega outside the earth's atmosphere based on irradiance calculated from visual and infrared magnitudes (Ramsey, 1962; Walker and D'Agati, 1964). Although the measured value is almost a factor of 2 higher than the predicted curve, the evidence was not deemed sufficient to assume that a responsivity change had occurred in the E3G-PMT channel.

5. EARTH-CLOUD RADIOMETRIC MEASUREMENTS

The long duration of the Gemini V flight provided the first opportunity for extensive earth-reflected sunlight measurements from a manned spacecraft. Data from the radiometer during the first two orbits while the filter wheel was operational showed no signal on the PMT and PbS channels and negative signals on the bolometer detector. Comparison of the bolometer outputs with the calibration curves reveals a target with a temperature colder than 77°K, and therefore it was assumed that the instruments were pointed into space. Once "frozen" on Channel 8, the 4000 Å channel was useless for earth measurements as it would saturate on the day side and be in the noise at night. The bolometer at 4.3μ was too insensitive to measure the earth's self-emission as planned (see Radiometer Calibrations, Appendix A). The 2.2-μ PbS channel was ideally suited for this type of measurement, and when used in conjunction with the I-14 interferometer provided a continuous monitor of earth-reflected sunlight in the 2.2-μ window.

A summary of the radiometric data is presented in Table 1 where the limits in intensity at 2.2μ for each target are shown graphically. Also included is the range of intensities encountered during the 14-day Gemini VII flight. Since the instrument field is completely filled during measurements of this type, the results are expressed in source radiance. The correlating information used in the last column was obtained from a voice recording of comments made by the astronauts and photographs taken with a 70-mm hand-held camera (Figures 6 and 7).

In general, the cloud cover during the Gemini V flight was heavier than that encountered on Gemini VII. This is reflected in the slightly higher radiance values obtained on this flight. Film coverage during the D4/D7 experiments is not as extensive as on the Gemini VII flight. This presents a severe handicap on data evaluation, since the target and spacecraft orientation is relatively unknown.

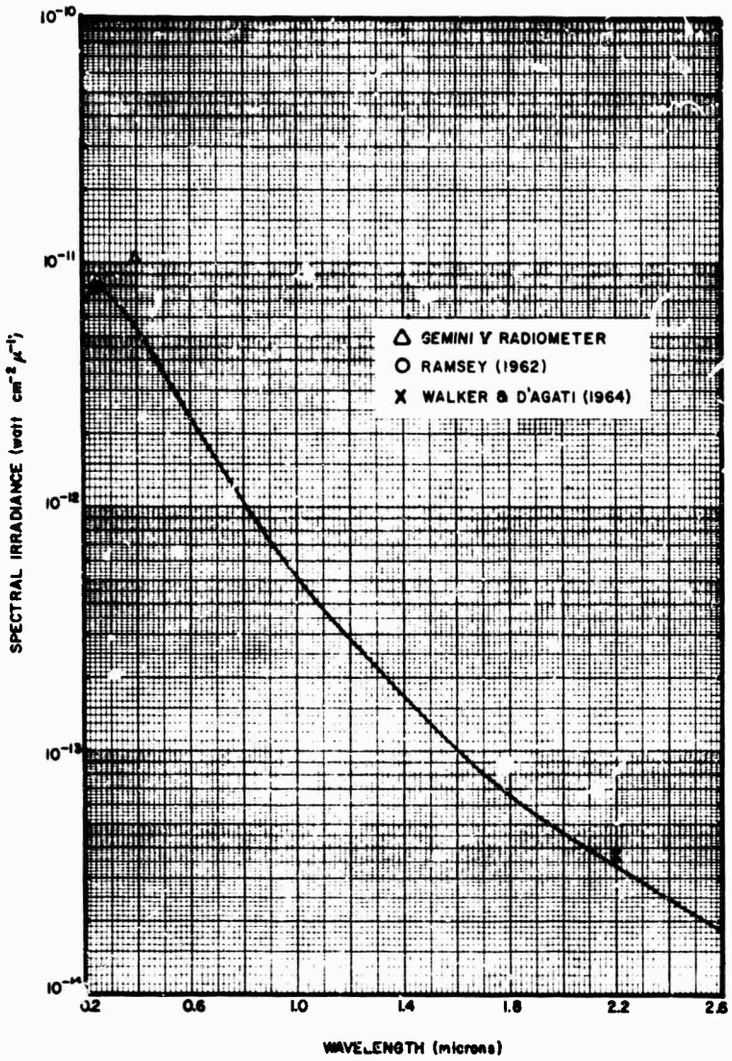

Figure 5. Radiometric Measurement of Vega Revolution 16

6. INTERFEROMETRIC DATA, REVOLUTION 47

Of the interferometric data received from the I-14 interferometer, two passes representative of the Gemini V earth background measurements are presented. The first during revolution 47 over the California coast, with simultaneous radiometric coverage, was recorded on the onboard tape recorder; in addition, numerous comments by the astronauts during the last half of the run provided valuable correlating information.

Table 1. Summary of Earth-Background Radiometric Measurements

Station	Orbit	Range in Spectral Radiance at 2.2 μ	Measurement* Start Time	Duration (min:sec)	Local Mean Time	Correlating Information
Kano	16		24:13:33	2:43	1100	No clouds visible to astronauts
Tananarive	16		24:32:30	2:29	1730	None
Texas	16		25:25:40	1:50	0540	Heavy cirrus and cumulonimbus clouds over Houston, Texas (see Figure 5)
Canaveral	16/17		25:33:00	4:00	0830	Cumulus clouds over Florida (see Figure 6)
Canaveral	31/32		49:18:00	7:00	0630	None
Tananarive	47		73:41:00	10:10	1700	None
California	47		74:36:00	5:00	1015	Clouds on water off California coast
Hawaii	51		80:44:50	5:00	1700	Graphic clouds over Hawaii Relatively clear ocean
Entire Flight of Gemini VII						

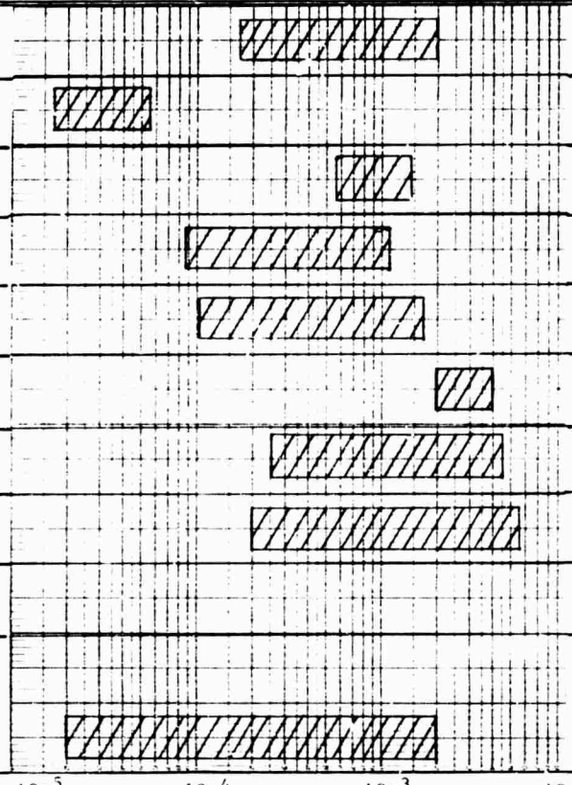

*Time unless otherwise specified will be ground-elapsed time in (hr:min:sec) where (00:00:00) represents the time at launch, 14 hr 00 min 00 sec GMT, 21 Aug 1965.

Figure 6. Heavy Cirrus and Cumulonimbus Clouds Over Houston, Texas

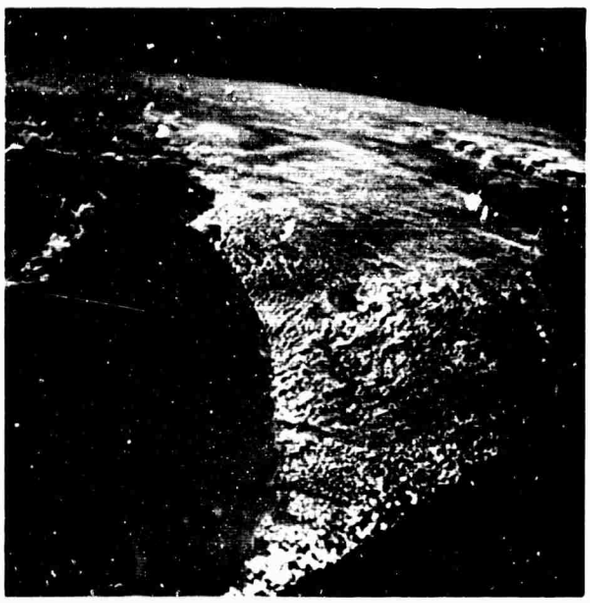

Figure 7. Cumulus Clouds Over Florida

A graphic comparison of the interferometric and radiometric data at 2.2μ is shown as a function of time for the entire pass (Figure 8). The dashed curve represents the PbS radiometer output reduced by a factor of 3.6 as described in the lunar measurements section. In order to make an exact comparison, the interferometer output was analyzed at a constant frequency of 707 Hz yielding the target radiance at 2.2μ. This wavelength was within the bandwidth of the I-14 filtered calibration lamp which added its signal to the target at approximately one-minute intervals.

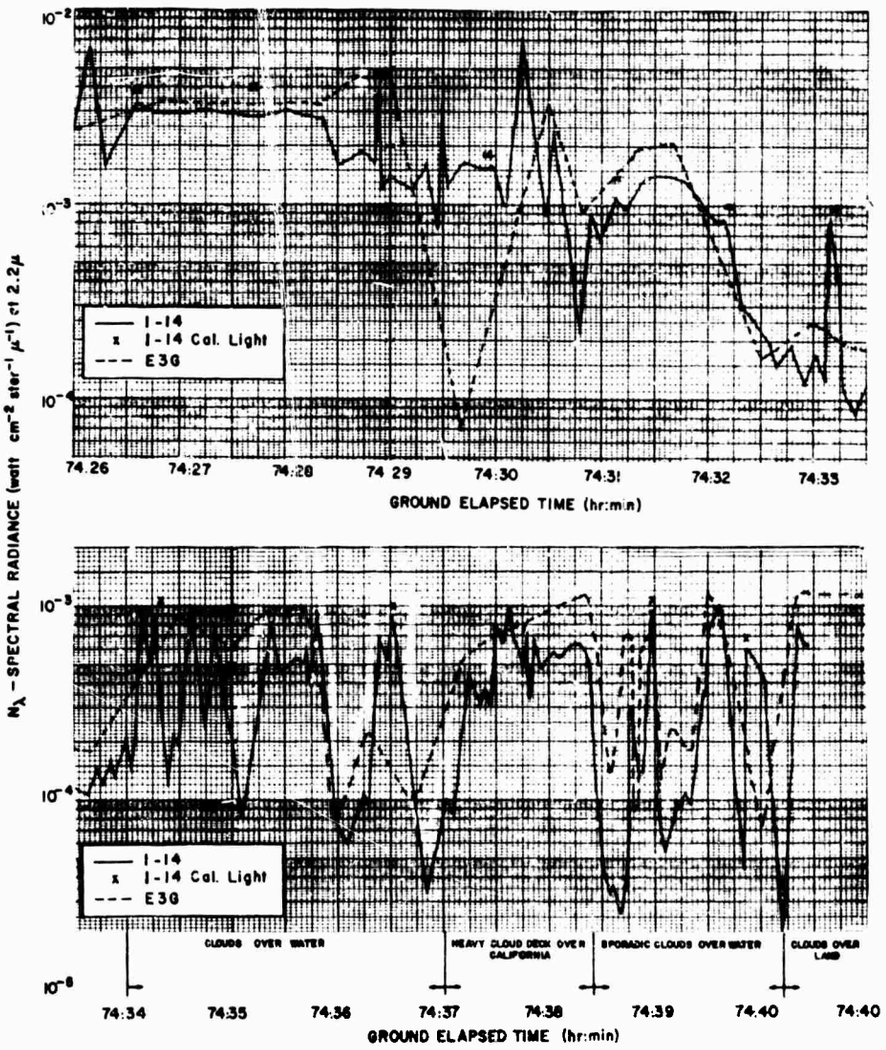

Figure 8. Spectral Radiance at 2.2μ vs Time (Calif. – Revolution 47)

A cross symbol on the figure is used to denote each such occurrence, and its effect should be discounted. The deviations in radiance level between the two instruments at any particular point in time is not surprising in view of the uncertainties in the alignment of the optical axes of the instruments. It is evident from the major changes, however, that the over-all targets were identical for both instruments, and it is this assumption that justifies the 3.6 reduction factor applied to the radiometric data.

The I-14 interferometric data were inferior to that obtained on Gemini VII for the following reasons: The PbS detector response was poorer in the 2.7μ region, the dichroic filter-beamsplitter attenuated the short wavelengths (1.0 to 1.5μ) more severely, and the noise level of the instrument output was higher across the entire spectral band. Nine analyzed spectra of earth reflected sunlight with various amounts of atmospheric absorption are shown in Figures 9 through 17. The solid portion of each curve is the actual data obtained from the Gemini V interferometer. The dashed portion represents the authors' best estimate of the remaining spectral distribution based on analysis of similar data from Gemini VII.

As in the case of Gemini VII, the absorption due to CO_2 remained relatively constant, whereas the amount of water absorption changed radically with cloud coverage. The only well-defined water absorption band was at 1.87μ and was used to estimate the attenuation in the other regions. Carbon dioxide absorption at 2.02 and 2.06μ was well defined in most of the spectra and enabled minor corrections in the ν/f value used during data reduction.

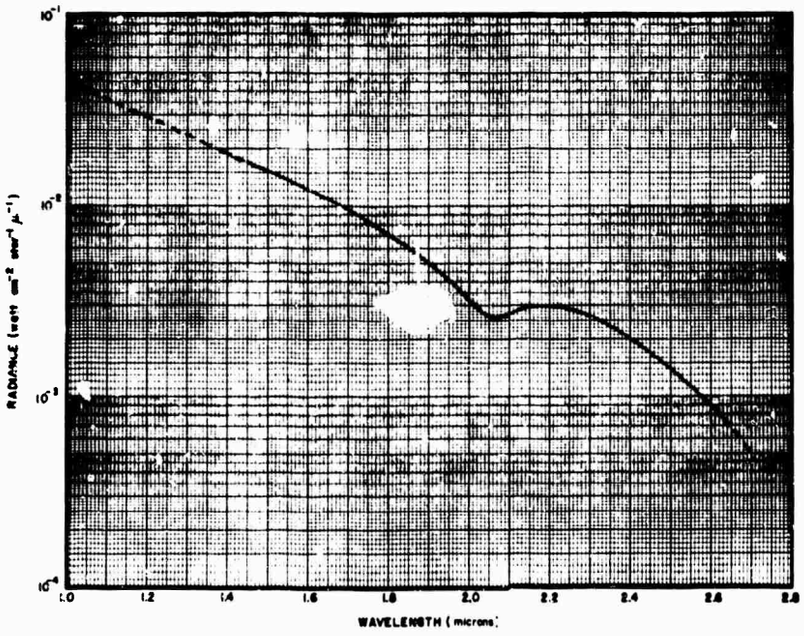

Figure 9. Revolution 47 – GET (74:27:57)

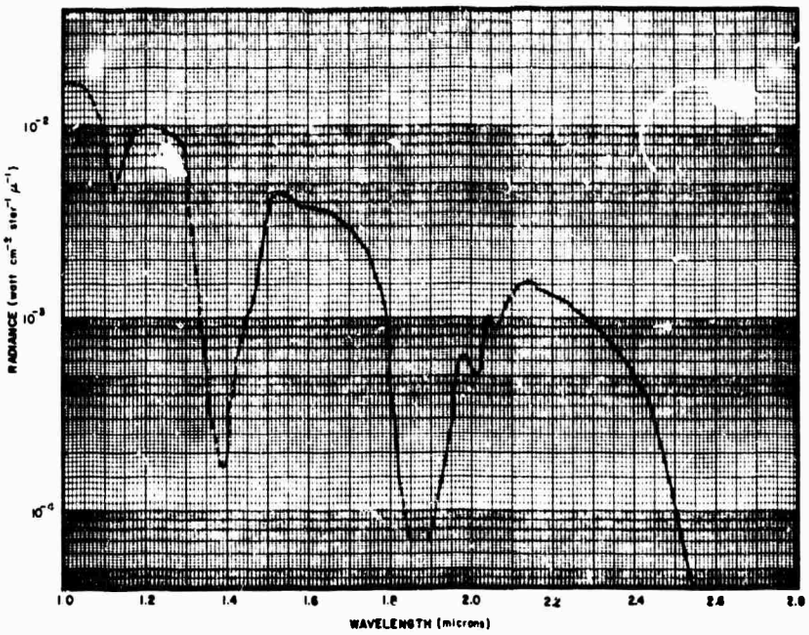

Figure 10. Revolution 47 – GET (74:31:30)

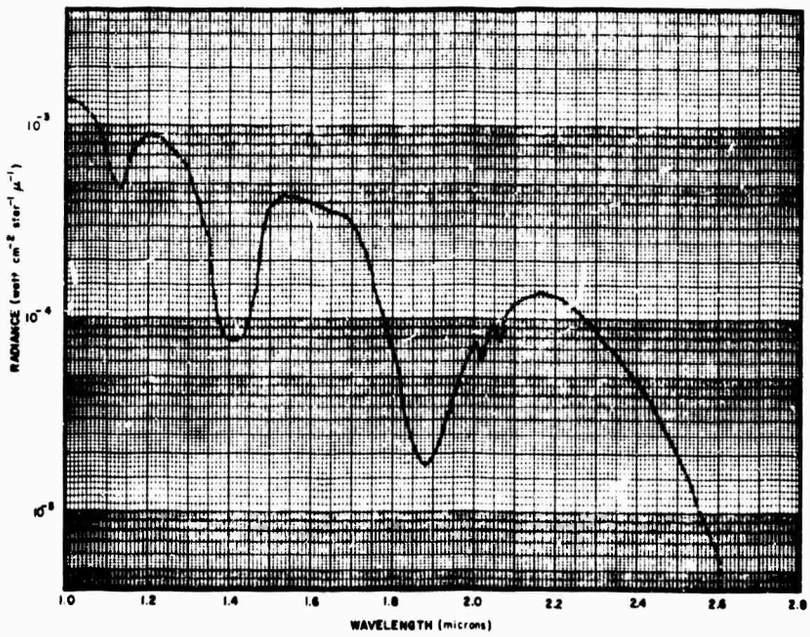

Figure 11. Revolution 47 – GET (74:32:48)

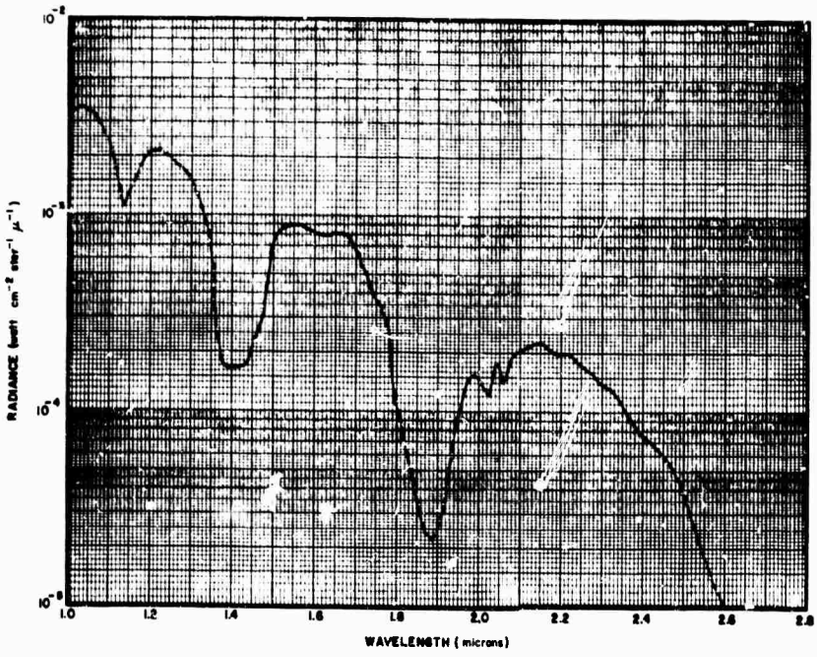

Figure 12. Revolution 47 – GET (74:34:02)

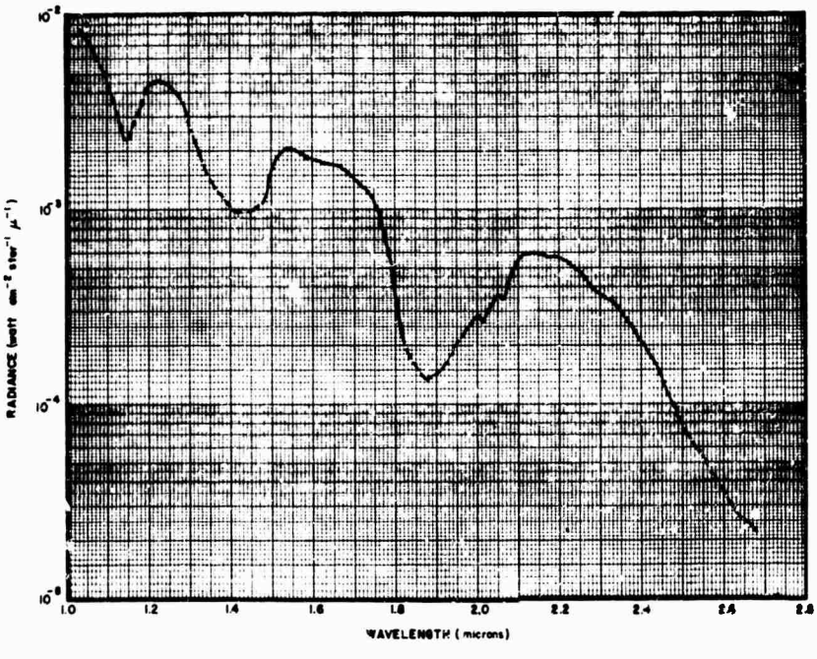

Figure 13. Revolution 47 – GET (74:34:14)

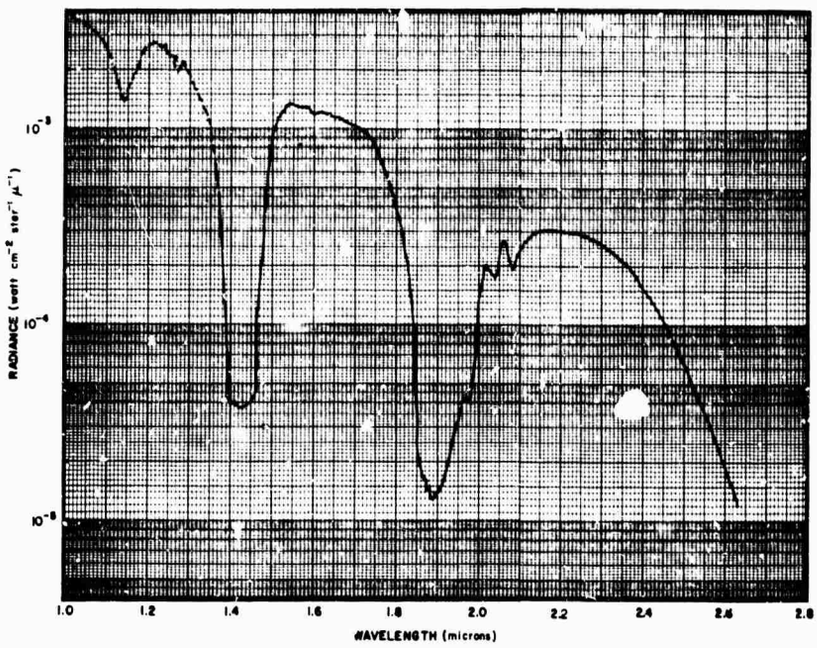

Figure 14. Revolution 47 – GET (74:37:26)

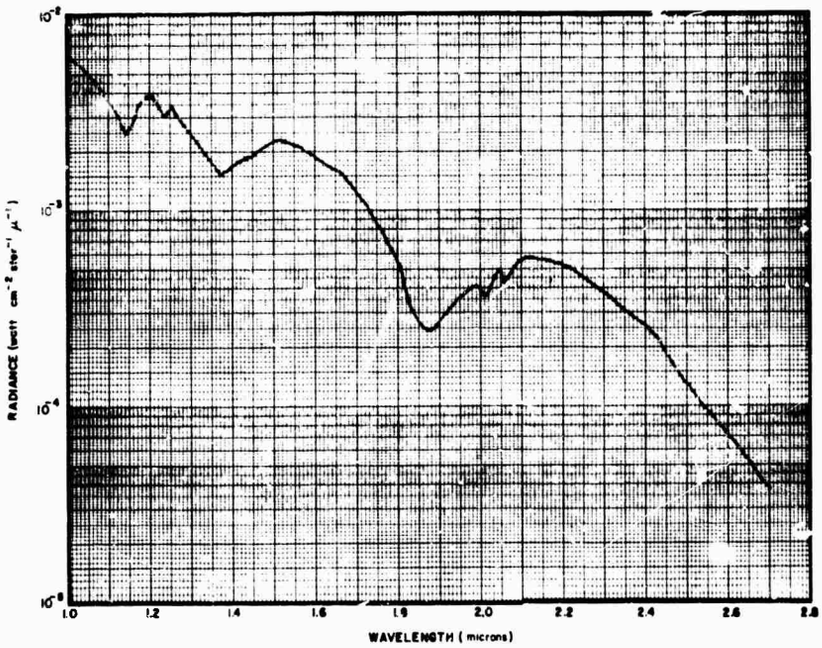

Figure 15. Revolution 47 – GET (74:38:00)

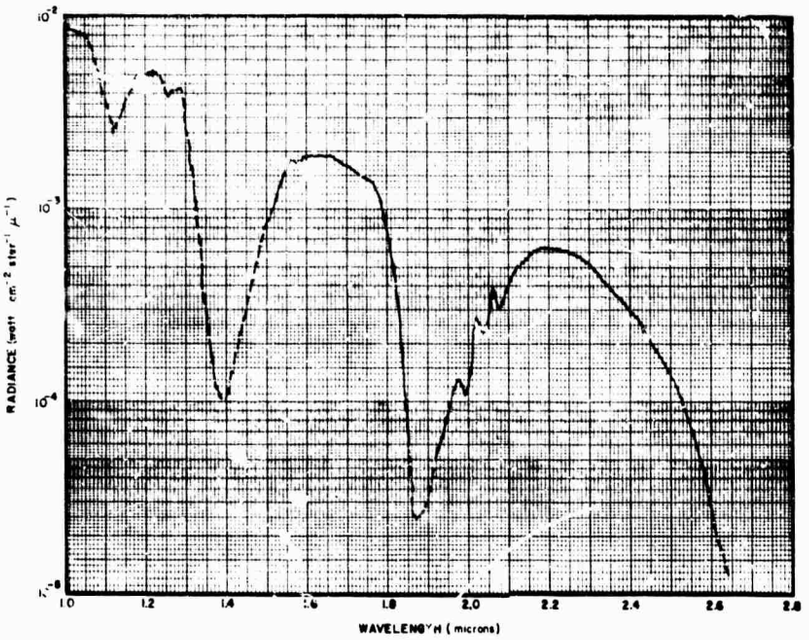

Figure 16. Revolution 47 -- GET (74:38:13)

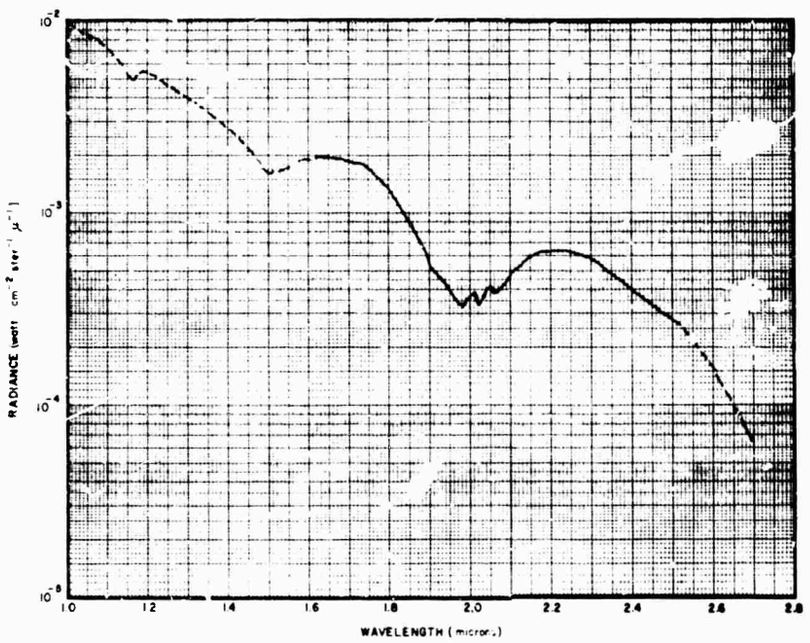

Figure 17. Revolution 47 – GET (74:40:25)

7. INTERFEROMETRIC DATA - HAWAII, REVOLUTION 51

Two photographs taken with the 70-mm hand-held camera during a pass over Hawaii provided invaluable correlating information for the spectral data taken on the fifty-first revolution. A plot of the spectral radiance at 2.2μ is shown in Figure 18 with comments on the nature of the target deduced from the photographs and remarks made by the astronauts. It is evident that the region prior to 80:47:20 has an appreciably lower radiance level. This is illustrated spectrally in Figure 19, taken as the spacecraft approached the Hawaiian Islands. The photograph in the figure was taken looking west a few minutes after the spectral measurement; it is included to show the relatively clear stretch of ocean traversed prior to the measurement made on the Islands.

Once in the vicinity of the island group, the astronauts kept the spacecraft pointed in the direction of the cloud-covered islands of Molokai and Hawaii by making corrections in attitude to compensate for their forward orbital motion. This portion of the measurement is typified by the spectrum shown in Figure 20. The photographic insert on the figure was taken along the axis of the spacecraft at the time of the measurement and shows the heavy cloud buildup associated with spectra of this type. Although the instrument field is not completely filled by clouds, their effect is evidenced by the higher over-all radiance level and the relative lack of water absorption.

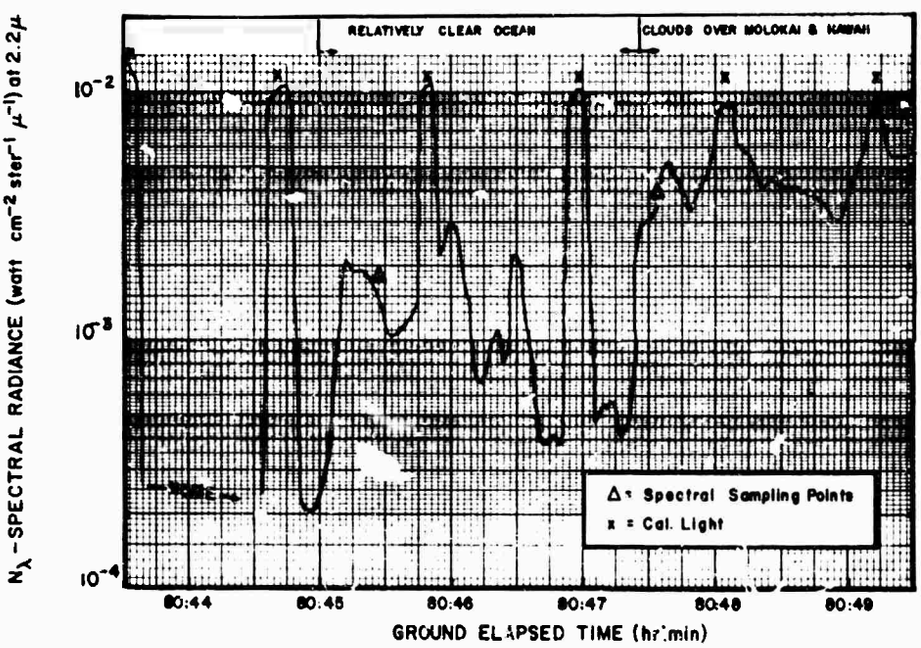

Figure 18. Spectral Radiance at 2.2μ vs Time (Hawaii – Revolution 51)

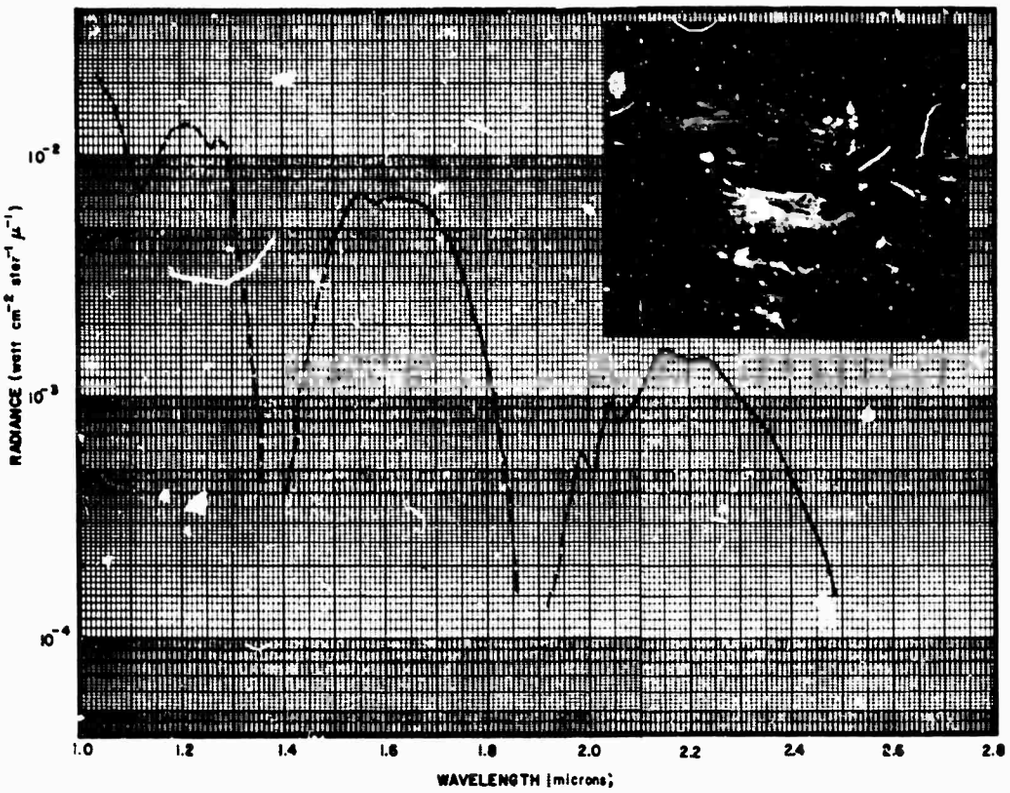

Figure 19. Hawaii Revolution 51 – GET (80:45:27)

8. CONCLUSIONS AND RECOMMENDATIONS

The measurements made on Gemini V though only partially successful were instrumental in the greater success of Gemini VII. As in the case of the latter, the CO_2 absorption remained relatively constant for all earth-cloud background measurements, whereas attenuation in the water bands was highly dependent on weather and topographical conditions. In general, the measurements made over large bodies of water through a cloudless atmosphere yielded spectra having the strongest absorption bands, whereas areas of high solid clouds displayed continuous spectra with little or no water absorption.

The short time interval between the launchings of Gemini V and VII placed a restriction on the changes that could be made in the instrumentation and measurement procedures. Although many improvements were made to good advantage, experience gained from both flights indicates the need for increased correlating in-

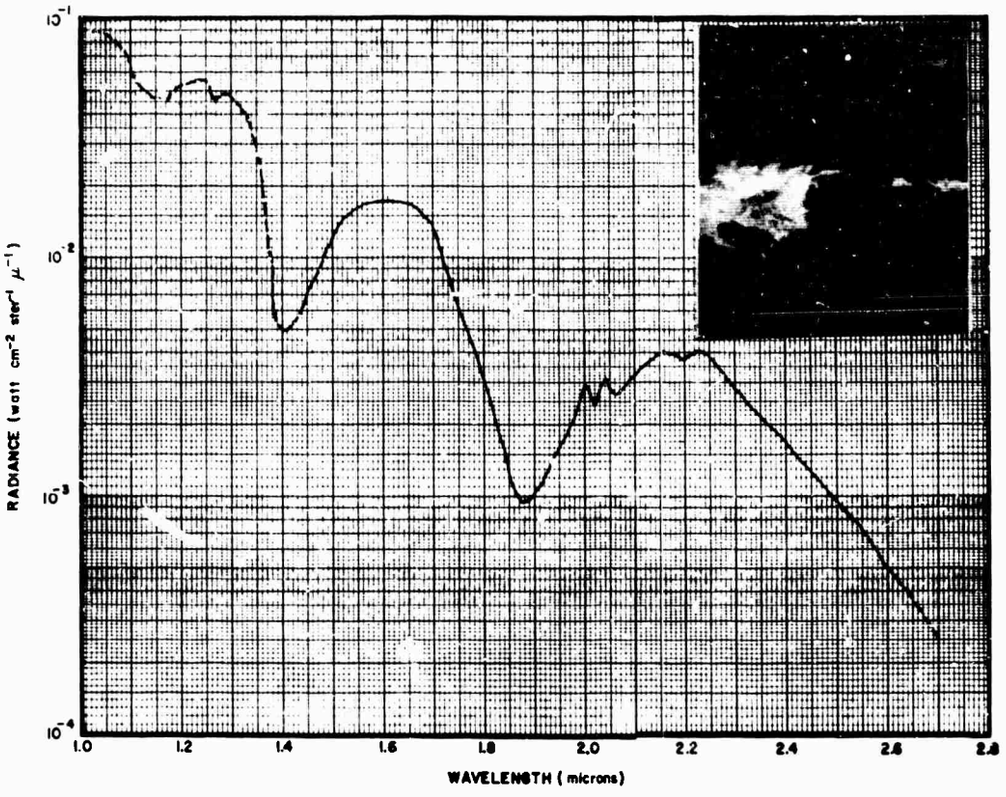

Figure 20. Hawaii Revolution 51 – GET (80:47:33)

formation and further refinement in the optical instrumentation. It is therefore recommended that future flights of this type make provision for the following:

1. Simultaneous photographic coverage with a boresighted camera which is automatically activated with the other instrumentation during each measurement.

2. Inclusion of a clock timer in the optical field of the camera to aid correlation with each data channel.

3. Recording of aspect data during earth-background measurements to allow accurate measurements of the attitude of the instruments relative to the solar incidence angle.

4. Provision for an inflight calibration source on each instrument.

Acknowledgments

The authors are particularly indebted to the following organizations and personnel: USAF Space Systems Division for their financial support and for the assignment of Major B. Brentnall to the project; NASA personnel at Houston, St. Louis, and Cape Kennedy whose excellent support and cooperation are sincerely appreciated; and ARPA for support in the reduction and analysis of the Gemini optical data.

They also acknowledge the following personnel who contributed a great deal of their time, effort, and skill in making the program a success: Warren Howell of Block Engineering Company for supervising the development and fabrication of the optical instruments; James Powers and David Newell of AFCRL for their excellent field engineering; Susan Flaherty of Boston College and John Winterbottom for their assistance in the reduction and drafting of spectral data.

The authors also express sincere appreciation to Gemini V Astronauts Gordon Cooper and Peter Conrad for their cooperation before, during, and after the flights and for accurate recording of personal observations which contributed significantly to the interpretation of the data.

References

Brentnall, B., and Lovett, J. (1966) Experiment D4/D7 Celestial Radiometry/ Space Object Radiometry, SSD-TR-66-130.

Condron, T., Lovett, J., Barnes, W., Marcotte, L., and Nadile, R. (1966) Gemini VII Lunar Measurements, AFCRL and Utah State University, Project Lamplighter.

Condron, T., and Nadile, R. (1966) Gemini VII Interferometer Calibrations, AFCRL and Utah State University, Project Lamplighter.

Nadile, R., Lovett, J., and Marcotte, L. (1967) Gemini VII Spectral Measurements of Space Objects and Earth-Cloud Backgrounds, AFCRL-67-0498, Paper No. 197.

Nadile, R., Turner, V., Marcotte, L., and Lovett, J. (1967) Gemini VII I-15 Cryogenic Interferometer Calibrations, AFCRL-67-0391.

Ramsey, R. (1962) Spectral irradiance from stars and planets, above the atmosphere, from 0.1 to 100.0 microns, Applied Optics, 1(No.4):465-471.

Struve, O. (1959) Elementary Astronomy, Oxford University Press.

Walker, R., and D'Agati, A. (1964) Infrared Stellar Irradiance, AFCRL-64-980; ERP 73.

BLANK PAGE

Appendix A

Gemini V Radiometer Calibrations

1. DESCRIPTION

The E3G Radiometer Serial 003 which was flown on Gemini V contained a 1P28 photomultiplier, a PbS detector, and a bolometer which provided three continuous channels of commutated data. A ten-position filter wheel which could be stepped by the astronauts in one of three modes was mounted in front of all three detectors, providing a total of 30 channels of information. Incoming radiation was collected by a 4-inch Cassegrain telescope which was boresighted to the axis of the spacecraft. One half of the collected power was diverted to the bolometer detector by a reflecting beamsplitter-chopper (Figure A1). The other half was transmitted to a front surface striped aluminum mirror which transmitted one quarter of the originally available power to the PbS detector through one of ten possible filter wheel apertures. The remaining 25 percent was reflected by the striped mirror through one of the photomultiplier filter wheel apertures to the 1P28 PMT detector.

The photomultiplier section of the Gemini V radiometer was equipped with an automatic four-step attenuator that allowed linear operation throughout its dynamic range, the attenuation factors being 1, 3.3, 12, and 40. The PbS section was equipped with a logarithmic amplifier designed to compress four decades of incident irradiance into a 4-volt output. An offset of 1.15 volts was provided to raise the output voltage for small signals to a level well above telemetry noise. The bolometer amplifier was also logarithmic and was provided with a 2.5-volt offset to allow measurement of targets that were colder than the ambient temperature of the instrument.

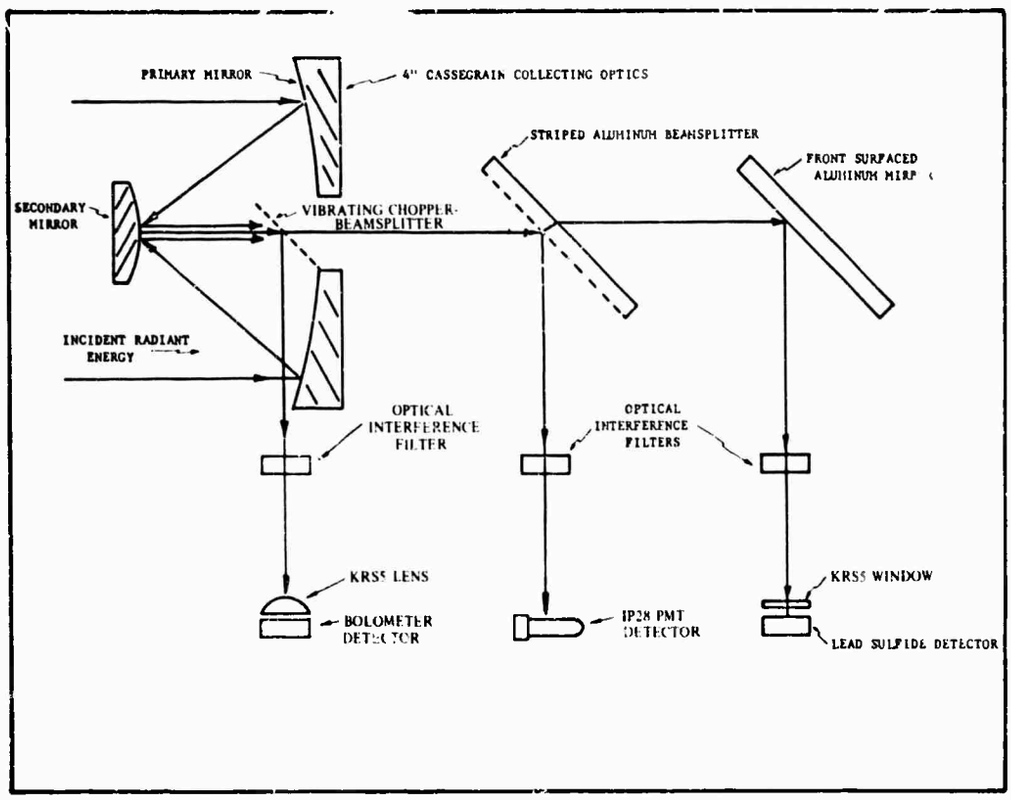

Figure A1. E3G Radiometer Optical Diagram

2. INSTRUMENT PARAMETERS

After 15 minutes of operation during the second revolution on Gemini V, the radiometer filter wheel ceased operation and remained on Channel 8 for the remainder of the flight. Analysis of the data prior to the inoperation of the filter wheel shows ambient noise level from the PMT and PbS detectors. Thus, this calibration will be concerned only with the channel 8 positions of these detectors which were filtered at 4000 Å and 2.2μ, respectively. The bolometer data during the second revolution show negative signals on some channels, and therefore a calibration of each bolometer channel is included.

Prior to a detailed discussion of the instrument calibration, a summary of the E3G's more significant parameters is included in Tables A1 and A2.

Table A1. E3G Radiometer Parameters, Channel 8

	PMT	PbS	Bolometer
Filter wavelength, λ_c	4030 Å	2.20μ	4.34μ
Filter transmission, t	0.295	0.445	0.552
Bandwidth, $\Delta\lambda$	240 Å	0.135μ	0.14μ
Field of view, w (ster.)	2.85×10^{-4}	2.44×10^{-4}	4.95×10^{-4}
Noise Equivalent Flux Density, NEFD (watt cm^{-2} μ^{-1})	3.0×10^{-12}	1.5×10^{-9}	4.95×10^{-7}
Noise Equivalent Spectral Radiance, NESR (watt cm^{-2} $ster^{-1}$ μ^{-1})	1.05×10^{-8}	6.16×10^{-6}	1.0×10^{-3}
Dynamic Range	1.3×10^{3}	3.0×10^{4}	6.0×10^{2}
Inverse Irradiance Responsivity, B	2.95×10^{-11}	...	...

Table A2. E3G Radiometer Filter Assignments

Channel	Photomultiplier		Lead Sulfide		Bolometer	
	λ_c (Å)	$\Delta\lambda$	λ_c (μ)	$\Delta\lambda$	λ_c (μ)	$\Delta\lambda$
1	4993	225	1.05	0.14	4.61	0.45
2	2690	300	1.26	0.14	6.03	0.42
3	3025	450	1.55	0.11	Open	....
4	2155	190	1.358	0.245	9.53	0.21
5	Blind	...	Blind	.....	Blind	....
6	2835	250	1.90	0.14	15.01	0.88
7	2400	300	2.707	0.118	Open	....
8	4030	240	2.20	0.135	4.34	0.14
9	6018	265	Open	....	9.57	1.72
10	3590	380	2.83	0.11	8.2 LWP	12.0

3. PHOTOMULTIPLIER RESPONSIVITY CALIBRATION

The ten PMT channels were calibrated absolutely by placing the instrument in the collimated beam of a 25-inch focal length, 6-inch diameter off-axis collimator manufactured by Infrared Industries, Inc. The radiation source was a 1/4-inch circular aperture 2000°C black body manufactured by Rocketdyne. Calibration points were obtained by rotating a precision aperture plate and varying source temperature. The threshold voltage, V_N, was subtracted from the instrument output, V_{T+N}, to arrive at the target voltage, V_T. Plots of V_T vs irradiance were then made. These plots showed that the photomultiplier section had a linear response for all attenuation settings and provided the attenuation factors. Thus, the conversion of target voltage to irradiance can be accomplished by an equation of the form

$$H_\lambda = B\, V_T\, a_m \qquad (1)$$

where

H_λ = spectral irradiance (watt $cm^{-2}\, \mu^{-1}$)
B = inverse irradiance responsivity (watt $cm^{-2}\, \mu^{-1}\, volt^{-1}$)
a_m = attenuation factor ($a_1 = 1.0$, $a_2 = 3.3$, $a_3 = 12.0$, $a_4 = 40.0$).

The irradiance calibration for Channel 8 is shown graphically in Figure A2 where V_T has been multiplied by the appropriate attenuation factor.

Each channel was checked for off-band spectral leakage with a series of Schott long-wave pass filters. Although some problems were encountered with the ultraviolet filters requiring doubling up on the 3200 and 2400 Å channels, the 4030 Å filter on Channel 8 provided sufficient off-band rejection for target temperatures as low as 1000°C. A plot of the spectral transmission of this filter is shown in Figure A3.

4. PbS RESPONSIVITY CALIBRATION

The ten lead sulfide channels were calibrated with the same collimator and source used for the photomultiplier section. Since the lead sulfide section was nonlinear by design, it was necessary to plot the output voltage as a function of incident irradiance. The target voltage, V_T, was determined by subtracting the 1.15-volt offset from the instrument output. A plot of V_T vs spectral irradiance for the 2.2μ filter in Channel 8 is given in Figure A4.

Unlike the rejection problems encountered in the ultraviolet, all the lead sulfide filters had sufficient rejection for the expected targets. The spectral response of the 2.2μ filter shown in Figure A5 had 5 orders of magnitude rejection outside the nominal passband.

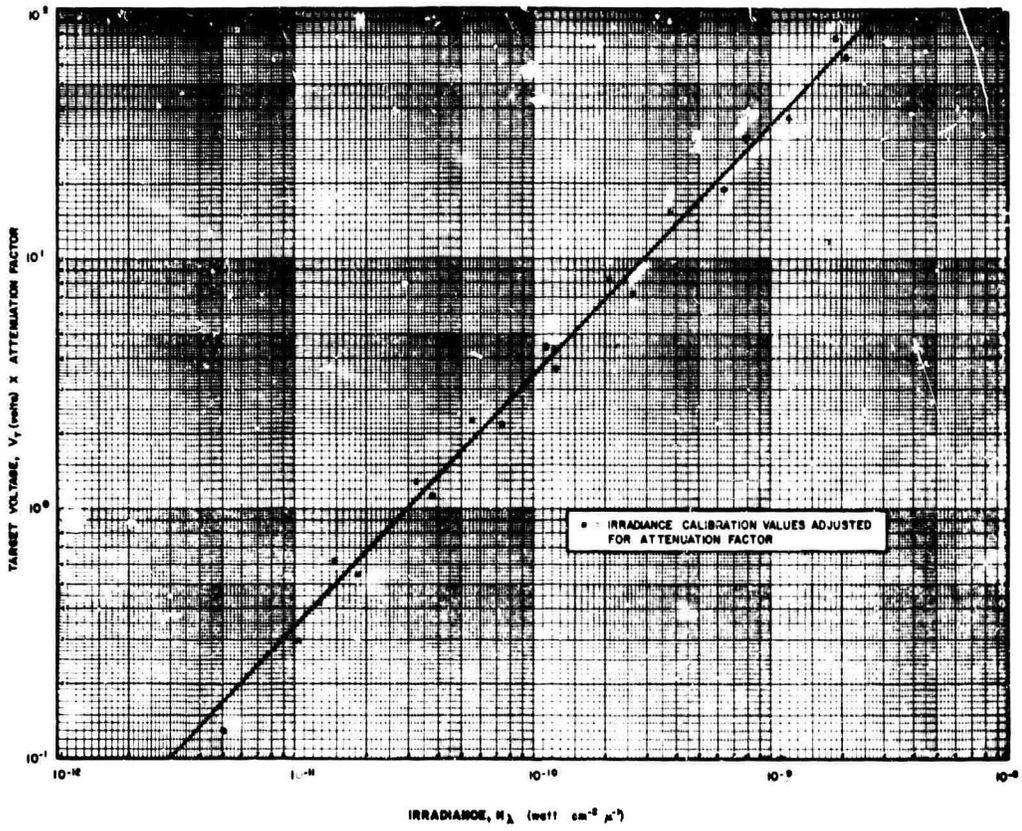

Figure A2. Photomultiplier Responsivity at 4030 Å (PMT-Channel 8)

5. VARIATION OF RESPONSIVITY WITH TEMPERATURE

The temperature of the E3G radiometer was monitored by four thermistors which were mounted adjacent to each of the three detectors and the instrument chopper. A plot of thermistor output, V_K, as a function of temperature is given for each thermistor in Figure A6. In order to provide coverage over a large temperature range, the operational ranges of the monitors were staggered.

Past experience has shown that the responsivity of a PbS radiometer varies considerably with temperature, and thus the irradiance given in Figure A4 applies only for calibration ambient conditions. Consequently, the responsivity as a function of temperature was determined by placing the instrument in an environmental chamber and varying the temperature while the instrument was irradiated with a constant source. A plot of responsivity vs temperature normalized to the temperature during calibration (22°C) is given in Figure A7. Thus, for instrument temperatures other than 22°C, the irradiance read from Figure A4 should be multiplied by

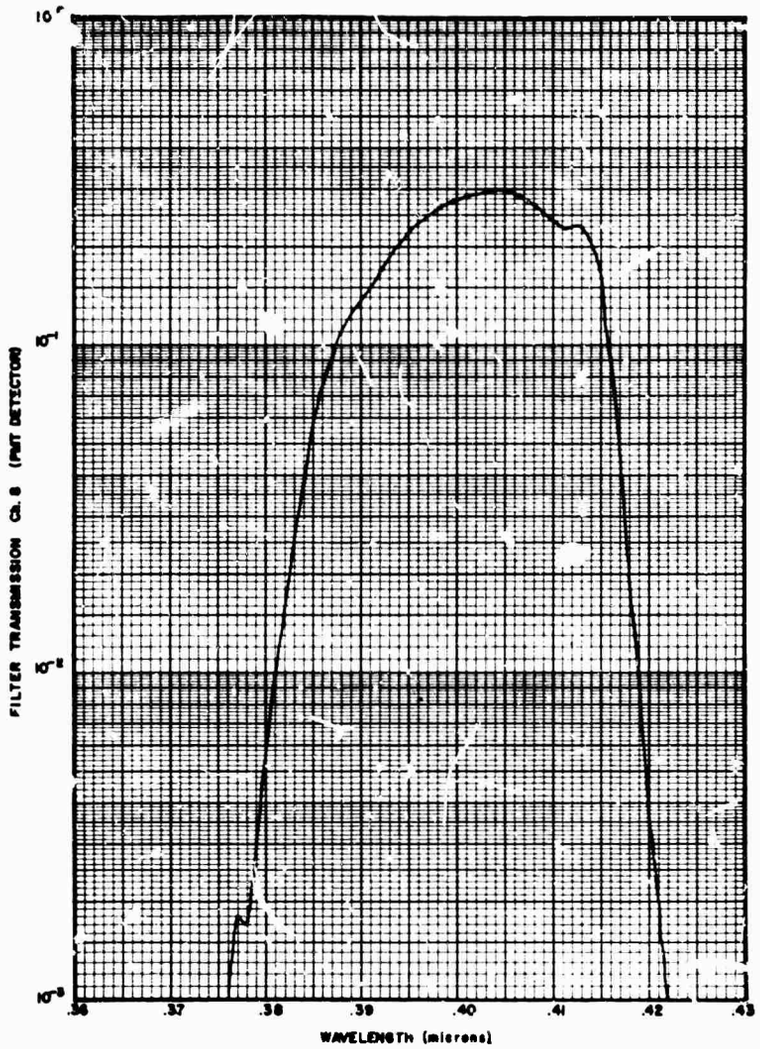

Figure A3. Spectral Transmission of 4030 Å Filter (PMT-Channel 8)

the temperature correction factor K to obtain the true irradiance at the instrument aperture. It is interesting that the PbS response goes through a maximum at −2°C, and the only explanation for this behavior is that changes in the characteristics of the log amplifier with temperature eventually cause an over-all decrease in system gain which counteracts the increased detector sensitivity as the temperature is decreased. All three E3G radiometers designed for the Gemini D4/D7 program exhibited this type of behavior.

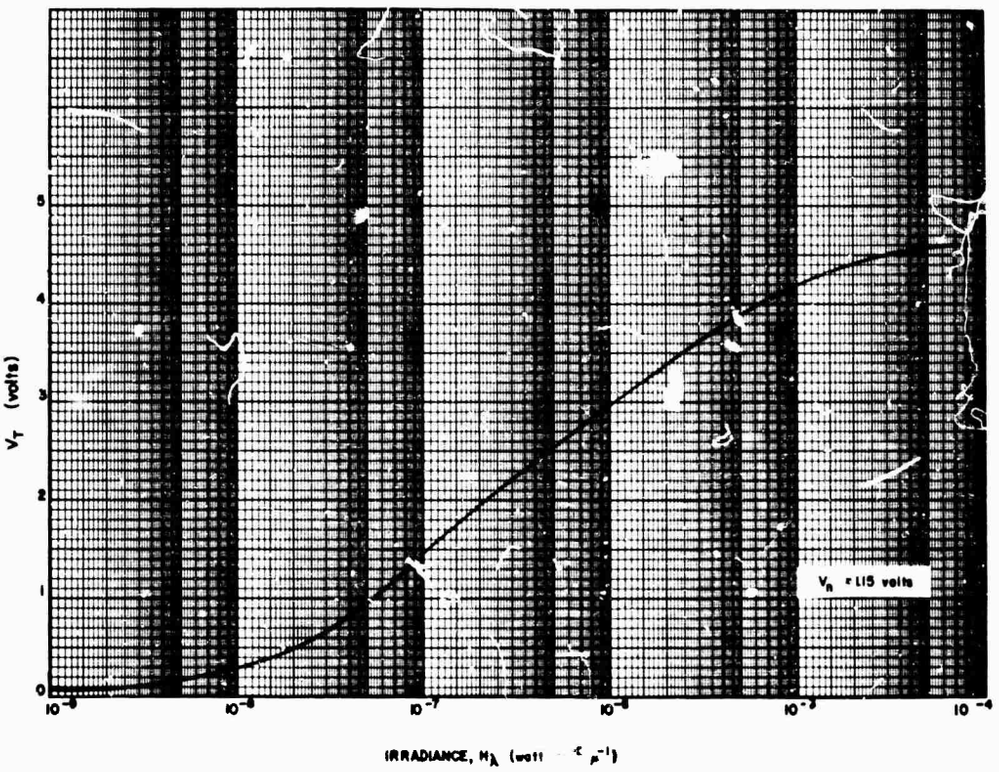

Figure A2. ..3C Radiometer Irradiance Responsivity at 2.2μ (PbS Channel 8)

The cha[illegible]e in responsivity due to temperature was negligible for the photomultiplier section, and no correction was applied to the PMT data. The bolometer responsivity on the filtered channels did not change significantly due to the negligible temperature difference between detector and filter. No correction was applied to the 20 seconds of unfiltered bolometer data, since the instrument field was filled by the void of space providing the expected negative saturation voltage.

6. BOLOMETER RESPONSIVITY CALIBRATION

Due to the insensitive nature of the bolometer detector, no collimated source was available which would utilize the dynamic range of the instrument. In lieu of this, the instrument field was filled by two calibrated extended sources whose temperature could be varied in known amounts over a 30° to 600°C temperature range.

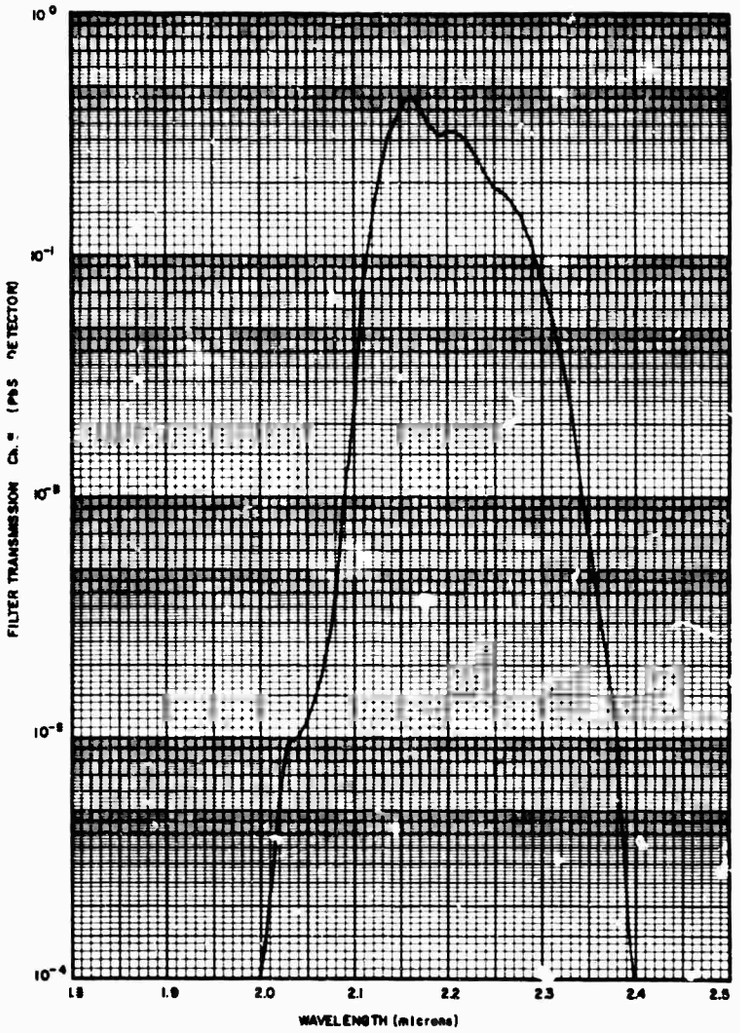

Figure A5. Spectral Transmission of 2.2μ Filter (PbS Channel 8)

A Lambertian radiating surface was assumed, and appropriate emissivity factors employed. Values of instrument output were then plotted against spectral radiance for each of the ten channels. The results are presented in Figures A8 through A12 by that portion of each curve which lies above the 2 5-volt offset level. All voltages below this offset were obtained by filling the instrument field with a blackened extended source cooled by liquid nitrogen. It is interesting that the shape of the response curve of each channel is so unique in view of the fact that all utilize the same detector and electronics. This is a result of the various filter bandwidths used, since the filter provides an additional source at wavelengths outside its

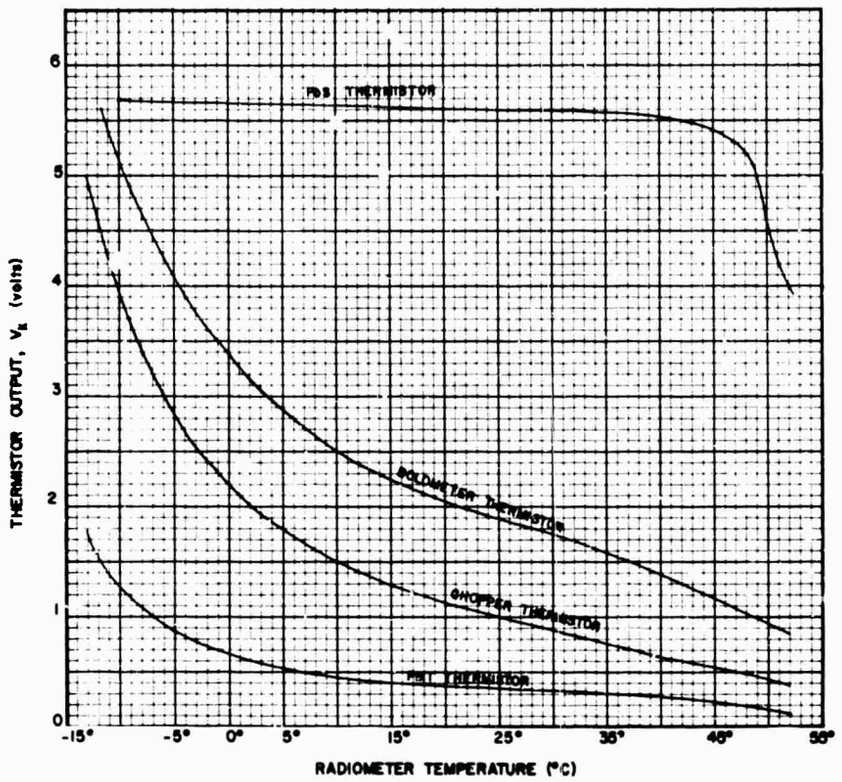

Figure A6. E3G Radiometer Thermistor Outputs as a Function of Temperature

transmission band. As an example, Figure A10 shows the response of Channels 8 and 9. The former at 4.3μ has a narrow bandwidth of 0.14μ (Figure A13) and hence is not very responsive to a change in spectral radiance. On the other hand, the latter with a bandwidth of 1.72μ at λ = 9.57μ shows a more reasonable change in outout as a function of radiance. From the foregoing, it was unfortunate from the point of view of the bolometer channel that the filter wheel "froze" on Channel 8. The radiance from the narrow band filter in this channel precludes any measurement of targets having temperatures colder than the radiometer filter.

Unlike the other filtered channels, Channels 3, 7, and 10 were not shown in terms of the target spectral radiance on a per micron basis because of the large bandwidths involved. Their outputs are plotted vs the total effective target radiance over the bandwidtn limits imposed by the instrument. For the open channels, an infinite bandwidth was assumed to be a reasonably accurate approximation for all expected target temperatures.

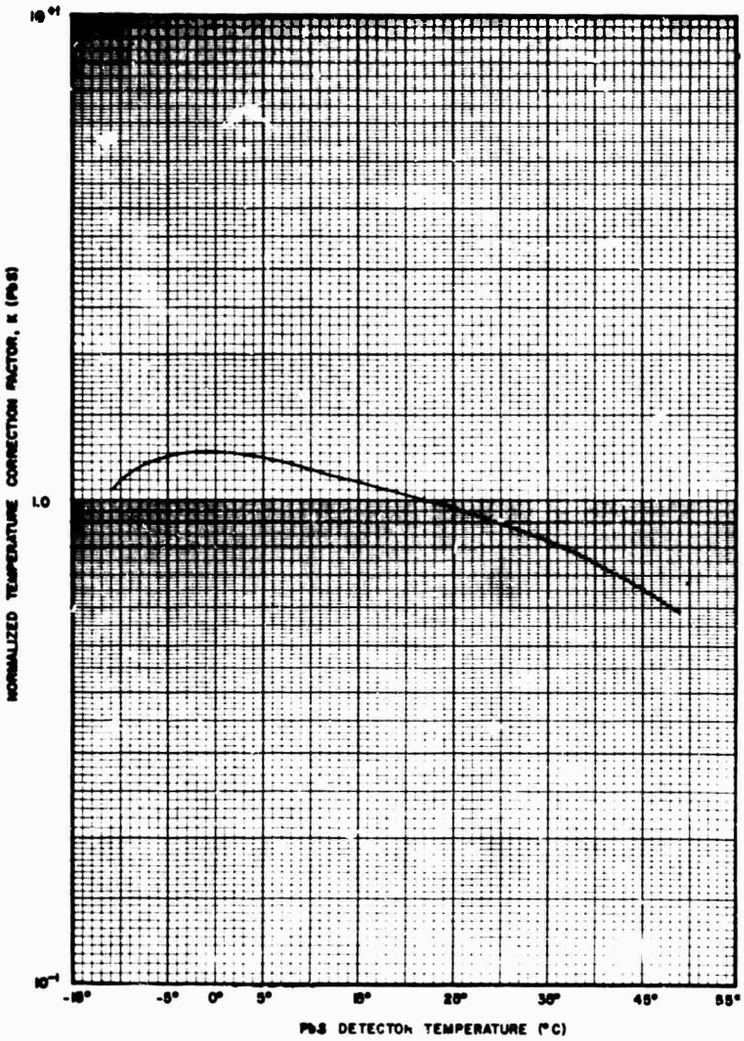

Figure A7. E3G PbS Normalized Temperature Correction Factor

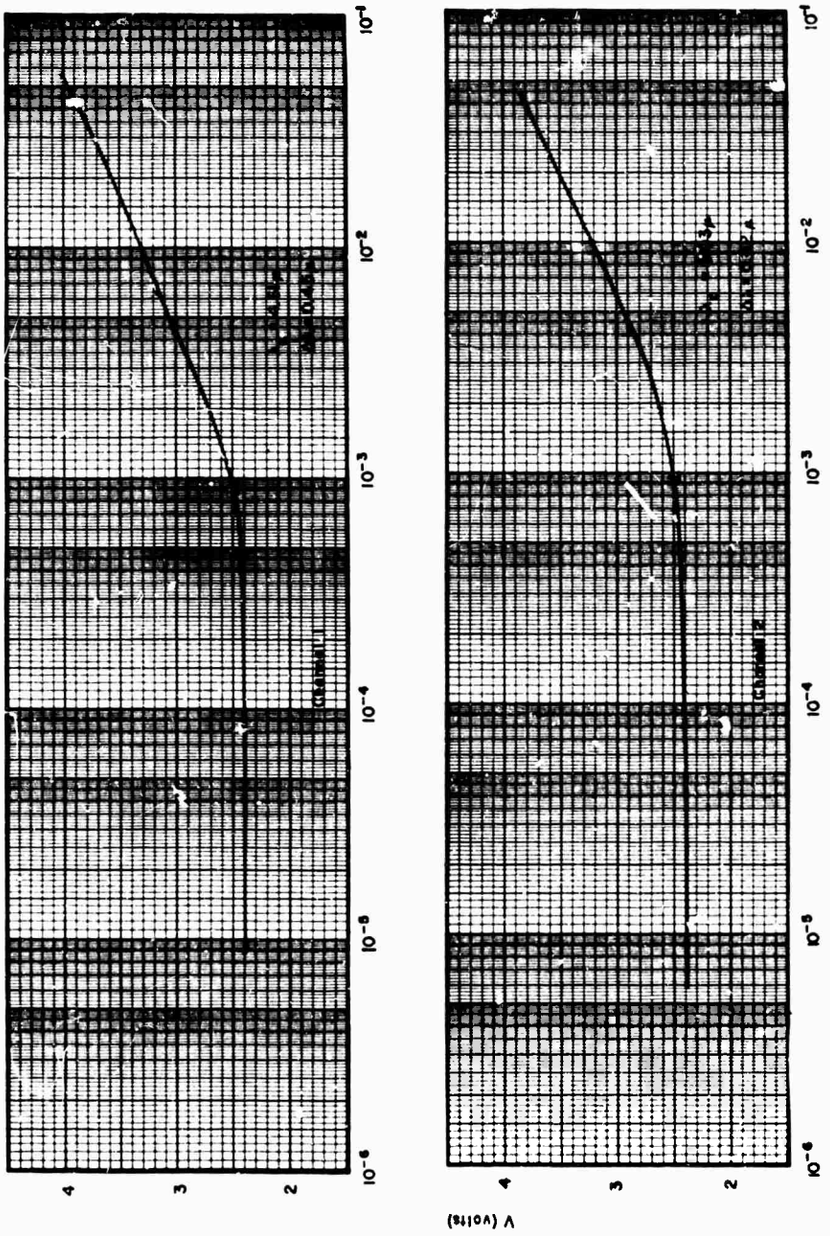

Figure A8. Bolometer Responsivity Channels 1 and 2

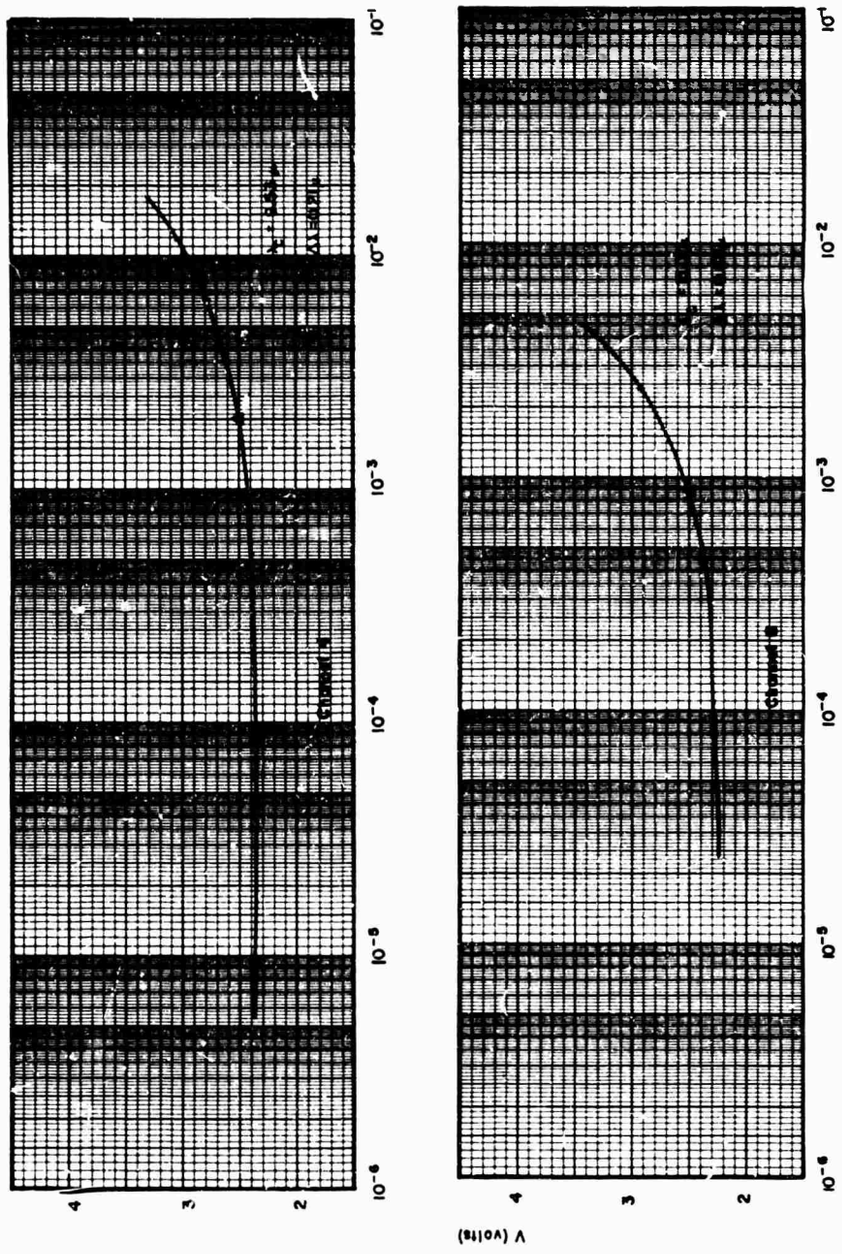

Figure A9. Bolometer Responsivity Channels 4 and 6

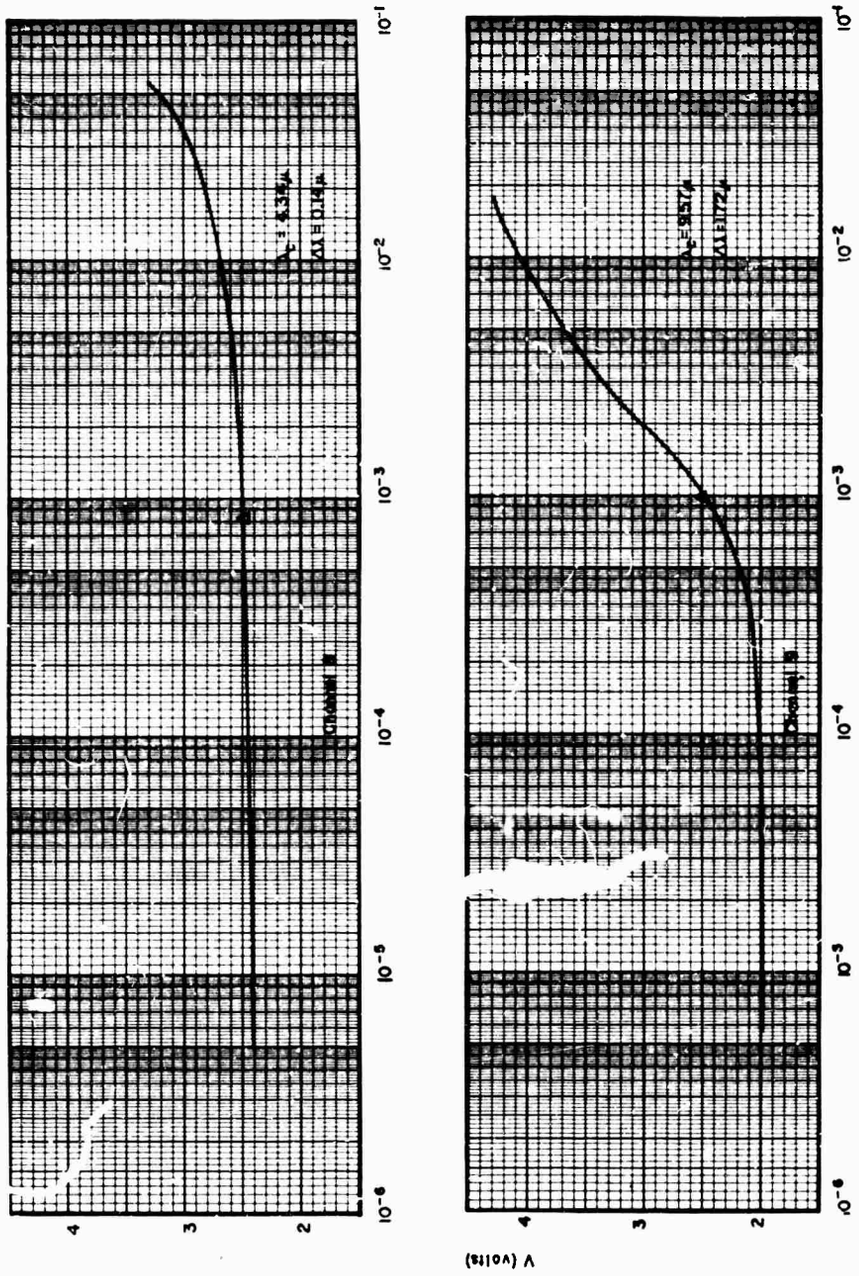

Figure A10. Bolometer Responsivity Channels 8 and 9

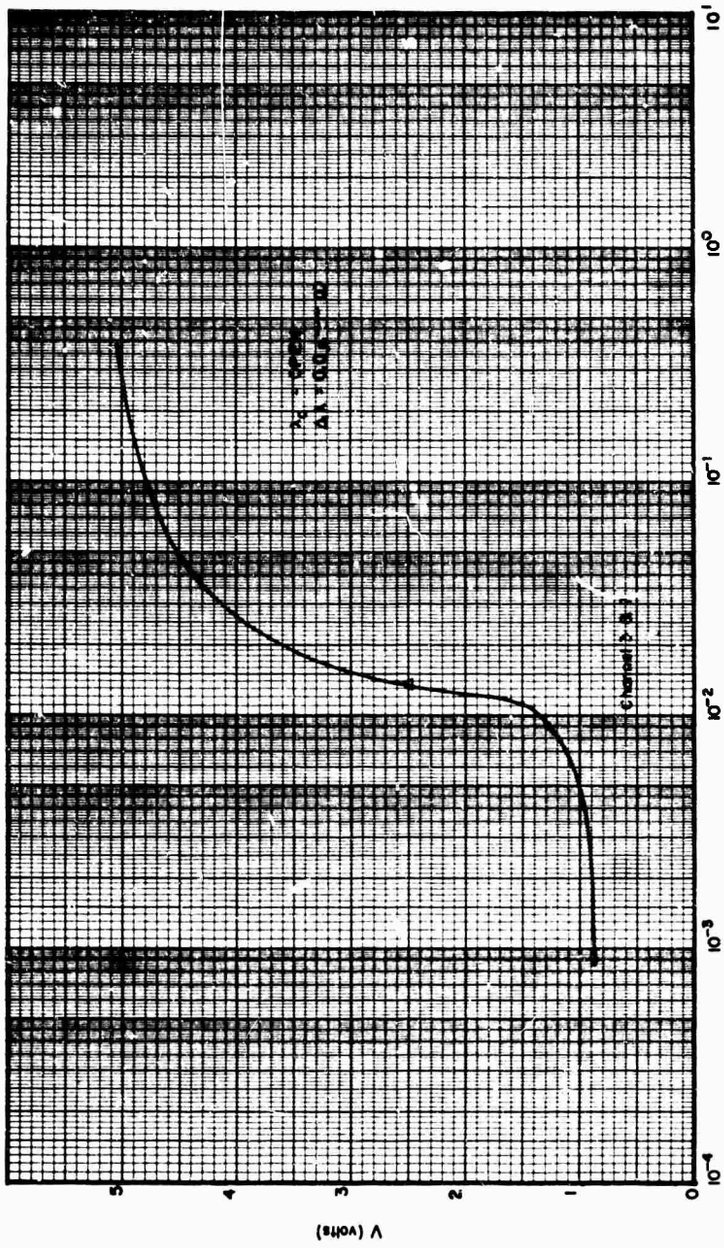

Figure A11. Bolometer Responsivity Channels 3 and 7

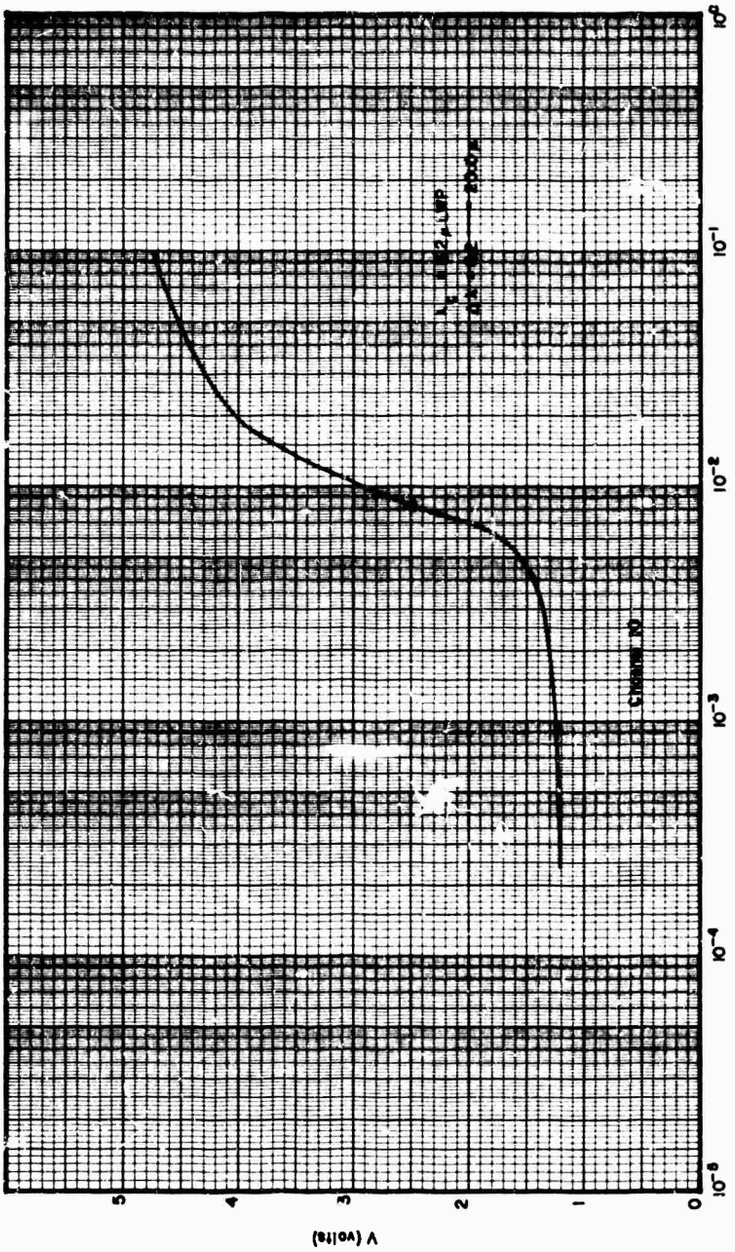

Figure A12. Bolometer Responsivity Channel 10

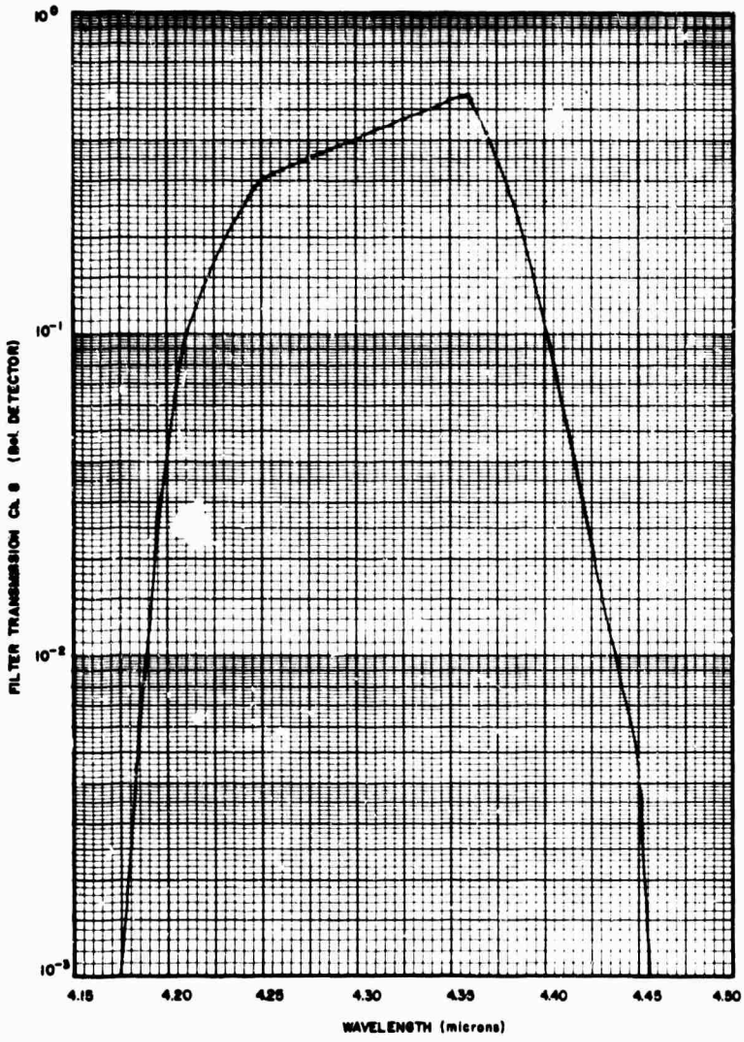

Figure A13. Spectral Transmission of 4.34μ Filter (Bolometer Channel 8)

7. FIELD OF VIEW

The field of view curves for the three radiometer sections are given in Figures A14, A15, and A16. These were measured by placing the instrument in collimated radiation and rotating it while the collimator remained fixed; the target used subtended an angle of approximately 0.005 radians, except in the case of the bolometer which required a larger aperture due to its insensitivity. Two orthogonal cuts were made for each channel; the solid lines on the graphs were made across

the longitudinal axis of the instrument, and the dotted lines were made orthogonally to the above. To ensure that the detector field of view was not affected by the filter selected, several fields of view were made on each detector. No variation with channel was found.

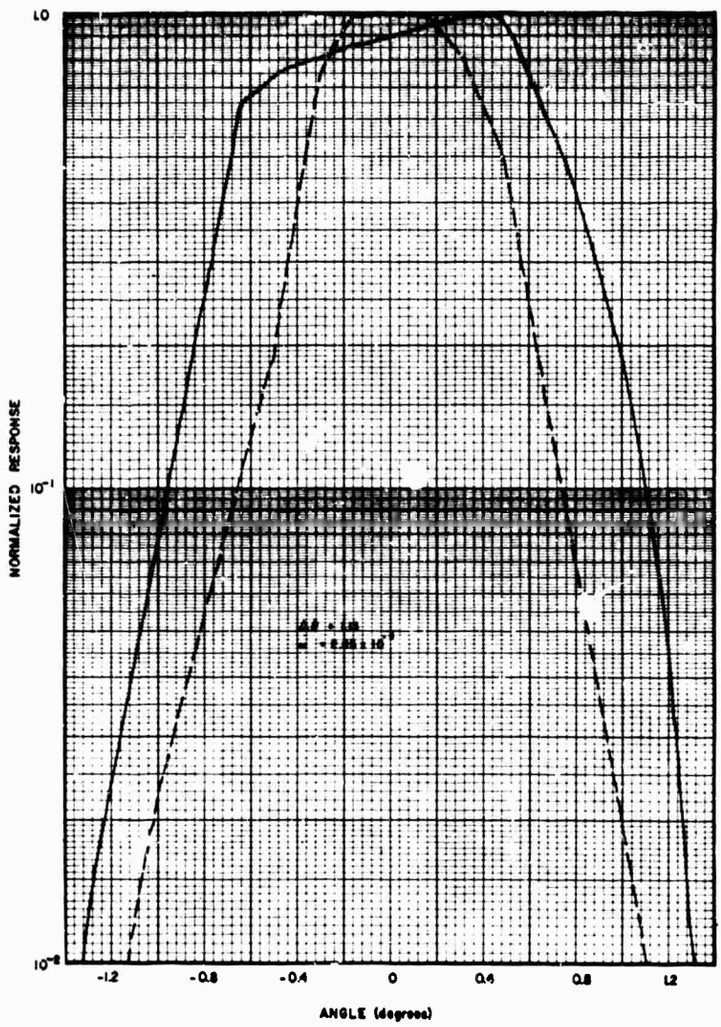

Figure A14. E3G EMT Channel Field of View

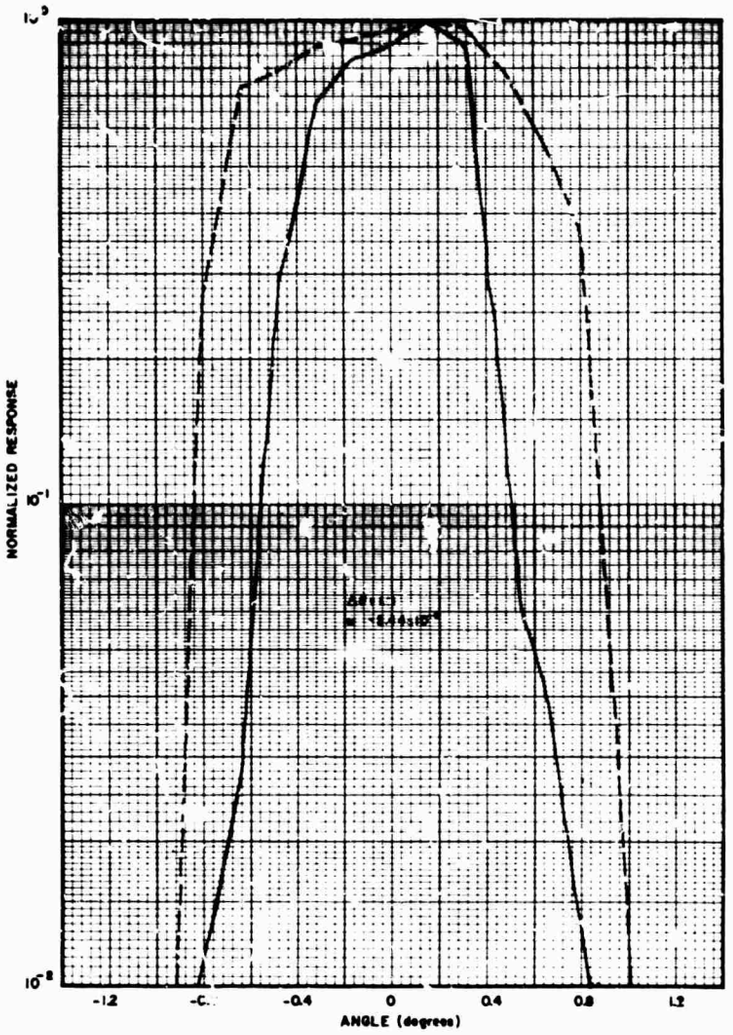

Figure A15. E3G PbS Cnannel Field of View

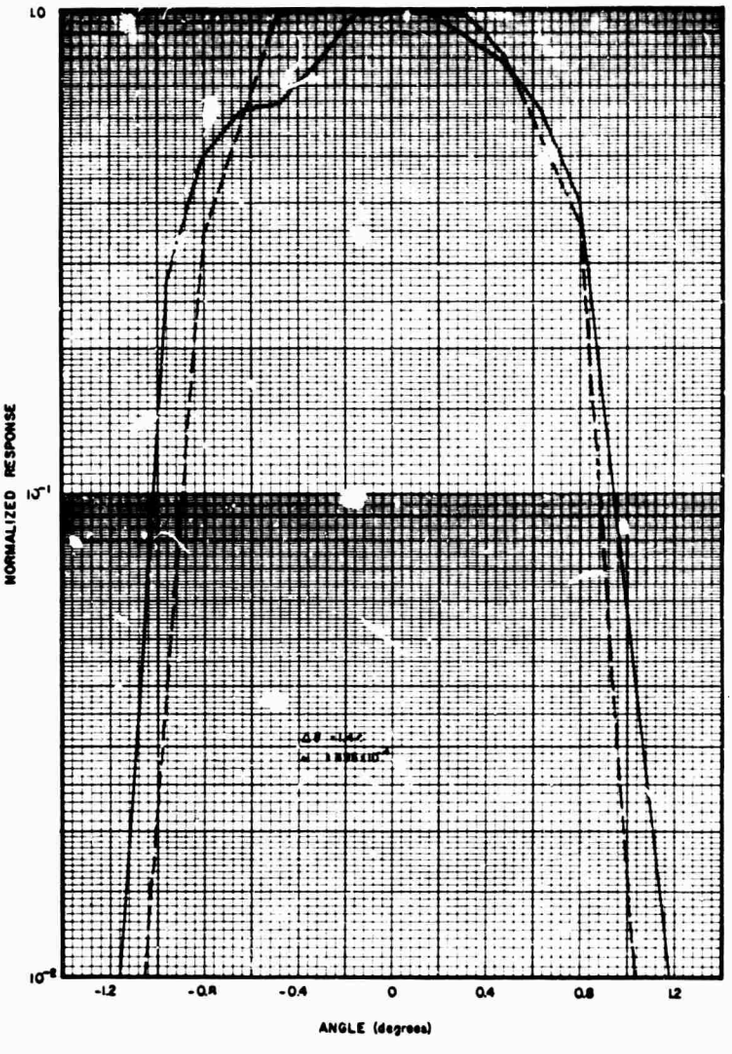

Figure A16. E3G Bolometer Channel Field of View

BLANK PAGE

Appendix B

Gemini V Interferometer Calibrations
I-14 Interferometer Serial 003

1. DESCRIPTION

The I-14 Interferometer Spectrometer was one of two Block Engineering rapid-scan Michelson interferometers mounted on the adapter section of the Gemini V spacecraft. This two-channel instrument was equipped with both a PbS and a bolometer detector that shared a common optical system and interferometer cube for spectral measurements in the 1.0 to 2.5 and 6.0 to 11.0μ regions. Both channels were provided with conical fields of view of approximately 2° in diameter in order to provide the best spatial resolution consistent with the sensitivity requirements imposed by the diverse targets.

A 4-inch Cassegrain telescope collected incident radiation which was channeled via a 45-deg angle mirror into the interferometer cube (Figure B1). The resulting interference pattern was directed to a dichroic beamsplitter which reflected 0.5 to 3.5μ radiation to the PbS detector and transmitted the longer wavelength radiation to the bolometer. The outputs of both detectors were fed to linear amplifiers equipped with four output attenuation settings which were switched automatically to accommodate the recording telemetry equipment. The attenuation settings were set so that the instrument signal outputs would not exceed 5.5 volts peak to peak while assuring that the noise level recorded on the onboard tape recorder would be the output of the interferometer.

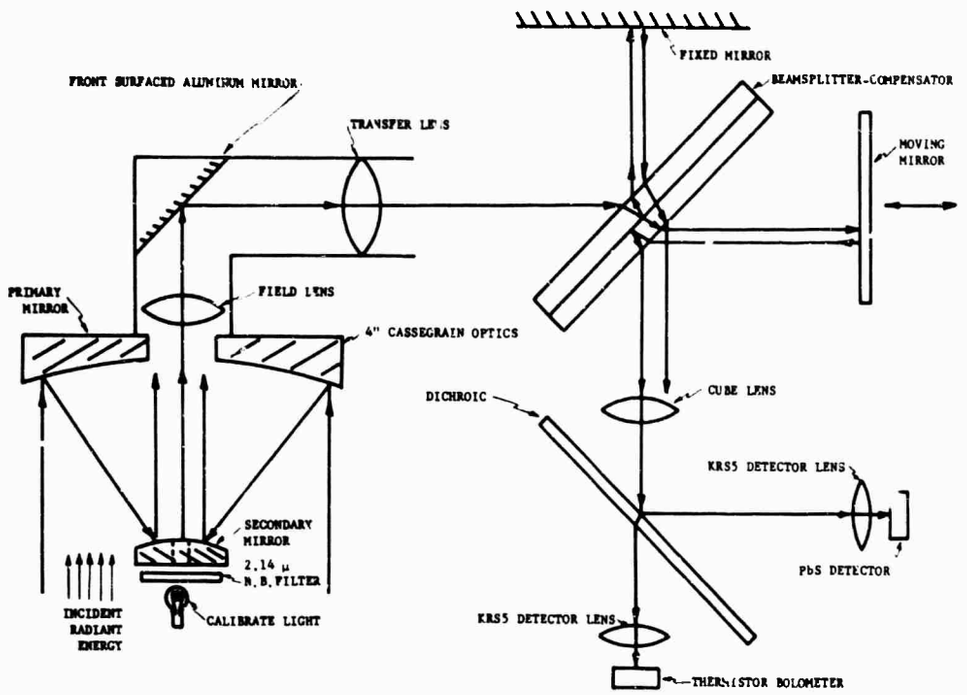

Figure B1. I-14 Optical Schematic Diagram

In addition to the signal outputs, the instrument was provided with binary-coded attenuation state monitors and two thermistors which measured the temperature at the two detectors. All outputs were commutated except for the signal channels which were recorded on an onboard recoverable tape recorder and simultaneously transmitted to ground stations within telemetry range of the spacecraft.

2. INSTRUMENT PARAMETERS

Prior to a detailed discussion of the instrument calibration, a summary of the more significant parameters of the I-14 Interferometer is included in Table B1.

For the purposes of this report, the radiance and irradiance responsivities are defined as follows:

$$\text{Radiance responsivity, } R_N = \frac{V_t}{N_\lambda} \tag{B1}$$

$$\text{Irradiance responsivity, } R_H = \frac{V_t}{H_\lambda} = \frac{V_t}{\omega N_\lambda} \tag{B2}$$

Table B1. Summary of Significant Parameters of the I-14 Interferometer, Serial 003

Optics (primary):	4-inch Cassegrain
Interferometer:	Michelson
Size:	Rectangular parallelepiped 15 × 7 × 9 in.
Dynamic Range:	300; in 4 automatic attenuation states
Output Signal:	Complex sinusoid to 5.5 v p-p
Optical Retardation:	668μ
Sweep Time:	430 msec
Spectral Resolution:	40 cm^{-1}
ν /f:	6.43 cm^{-1}/Hz
PbS Detector	
Spectral Region:	1.0 to 2.6μ
Frequency Range of Output:	600 to 1350 Hz
Spatial Resolution:	1.55 deg (5.67×10^{-4} ster)
Responsivity (radiance), * R_N:	8.95×10^{7} μV/watt cm^{-2} $ster^{-1}$ μ^{-1}
Responsivity (irradiance, * R_H:	1.58×10^{11} μV/watt cm^{-2} μ^{-1}
Noise Equiv. Spectral Radiance*:	7.0×10^{-6} watt cm^{-2} $ster^{-1}$ μ^{-1}
Noise Equiv. Flux Density*:	4.0×10^{-9} watt cm^{-2} μ^{-1}
Bolometer Detector	
Spectral Region:	6 to 11μ
Frequency Range of Output:	120 to 350 Hz
Spatial Resolution, ω:	2.01 deg (9.66×10^{-4} ster)
Responsivity (radiance), * R_N:	3.72×10^{6} μV/watt cm^{-2} $ster^{-1}$ μ^{-1}
Responsivity (irradiance), * R_H:	3.85×10^{9} μV/watt cm^{-2} μ^{-1}
Noise Equiv. Spectral Radiance*:	7.47×10^{-4} watt cm^{-2} $ster^{-1}$ μ^{-1}
Noise Equiv. Flux Density*:	7.22×10^{-7} watt cm^{-2} μ^{-1}

*These sensitivity parameters apply to the wavelength of peak detector response, that is, 2.4μ (PbS channel) and 9.0μ (bolometer channel).

where:

N_λ is the radiance of a target filling both the aperture and field of view of the instrument and is expressed in watts cm^{-2} $ster^{-1}$ μ^{-1}.

H_λ is the irradiance from a point source target at infinity producing collimated radiation that fills the instrument aperture and is expressed in watts cm^{-2} μ^{-1}.

ω is the effective instrument field of view in steradians which is limited by the field stop in front of the field lens and is defined as

$$\omega = \frac{\text{area of field stop}}{(\text{primary focal length})^2} \tag{B3}$$

V_t is the rms target voltage in microvolts within a 5-Hz bandwidth adjusted for the attenuation setting to its equivalent at the most sensitive gain state.

Use of the linear responsivity equations reduces accuracy when the output voltage, V_{t+n}, approaches the electronic noise of the instrument; therefore, the instrument electronic noise, V_n, is subtracted, assuming a random phase distribution relative to the target voltage. Thus,

$$V_t = a_m \left(V^2_{m(t+n)} - V^2_{m(n)} \right)^{1/2} \tag{B4}$$

where m is the attenuation state and a_m is the appropriate attenuation factor from Table B2.

Table B2. I-14 Attenuation State Factors

	PbS	Bolometer
a_1	1.00	1.00
a_2	3.54	3.62
a_3	11.0	....
a_4	36.3	....

3. INTERFEROMETER ν f CALIBRATION

The interferometer itself was a standard Block Engineering rapid-scan Michelson operating over a bandwidth of 1400 Hz and having an optical retardation of 668μ. In order to convert the sonic frequency (f) observed at the instrument output to the wavenumber (ν) of the incident radiation, the ν/f factor which is inversely proportional to the mirror velocity must be determined. This was accomplished by introducing CO_2 and H_2O in the optical path between a source and the instrument optics. The double CO_2 absorption bands at 2.02 and 2.06μ were used to determine the ν/f factor and spectral resolution of the PbS channel while the CO_2 and water absorption at 4.3 and 6.3μ provided the calibration of the bolometer channel. As expected, the ν/f and resolution parameters were identical for both detectors; a ν/f constant of 6.43 cm^{-1}/Hz and a resolution of 40 cm^{-1} were obtained during the calibration. Since all reduced interferometer data is expressed in terms of wavelength to facilitate comparison with the radiometric data, the product of frequency and wavelength is a more useful parameter and can be expressed as

$$f\lambda = \frac{10^4}{\nu/f} = \frac{B}{T} \mu Hz \qquad \text{(B5)}$$

where

ν = wavenumber in cm^{-1}
f = frequency in Hertz
λ = wavelength in microns
B = optical retardation in microns
T = period of mirror sweep in seconds.

The constant, $f\lambda$ for the I-14 during calibration was 1.555×10^3 μHz.

Experience with interferometers of this type has shown that the ν/f factor can drift as much as 7 percent in six hours. This is a slow monotonic drift which seems to correlate some degree with temperature. The problem is recognized by the manufacturer, Block Engineering, who usually provides a low-level oscillator and an inflight filtered calibration source to monitor the gain and ν/f of the system. The former has not been found particularly useful since it does not monitor the optical components of the system. The filtered calibration lamp located on the secondary of the Cassegrain system has been used on several interferometers of this type and has proved to be the most useful device for checking inflight instrument parameters.

4. PbS SPECTRAL RESPONSIVITY CALIBRATION

Calibration throughout the dynamic range of the PbS portion was performed using a 60-inch focal length collimator manufactured by Barnes Engineering and a 2000°C Rocketdyne 1/4-inch black body source. The instrument output voltage as a function of irradiance was determined at several wavelengths throughout the band by changing the aperture size and source temperature settings. The linearity of instrument response for each attenuator state was verified, and the attenuation factors a_m were determined and proved to be invariant with wavelength. The convention of labeling the most sensitive of the four instrument states as attenuation state number one has been adopted. Thus, for the lead sulfide channel, the instrument output in states 2, 3, and 4 must be multiplied by the factors 3.54, 11.0, and 36.3, respectively, when used in the responsivity equations.

Once the attenuation factors were determined, a complete spectral calibration was performed at wavelength increments smaller than the resolution element of the instrument. Interferograms from each of several targets were analyzed with a Technical Products Wave Analyzer employing a scanning electronic filter with a 5-cycle bandwidth. Computerized reduction utilizing Eqs. (B2) and (B4) yielded a family of spectral irradiance responsivity curves with an over-all variation of 10 percent in the region of maximum response. The average of these curves is shown in Figure B2 and is the responsivity which was used to reduce the Gemini V flight data.

The instrument sensitivity was limited by the electronic noise level which was a function of wavelength and attenuation state. Figure B3 shows a plot of the four electronic noise levels with $V_{m(n)}$ corrected to the most sensitive state to be compatible with the responsivity curve. A graph displaying the instrument noise equivalent flux density in its most sensitive configuration is shown in Figure B4. It should be noted that the attenuation setting is controlled by the over-all intensity of the incident radiation in the 1.0 to 2.6μ region, regardless of the spectral distribution within the band. Therefore, the sensitivity at a particular wavelength can be forcibly reduced by a strong signal in another portion of the spectrum.

5. BOLOMETER SPECTRAL RESPONSIVITY CALIBRATION

Calibration of the bolometer channel was accomplished using methods similar to those described above. Due to the relative insensitivity of the bolometer detector, however, it was necessary to use extended sources which filled the instrument field of view. Thus, the irradiance responsivity of Eq. (B2) was determined by using the radiance of the black-body source in conjunction with the bolometer field

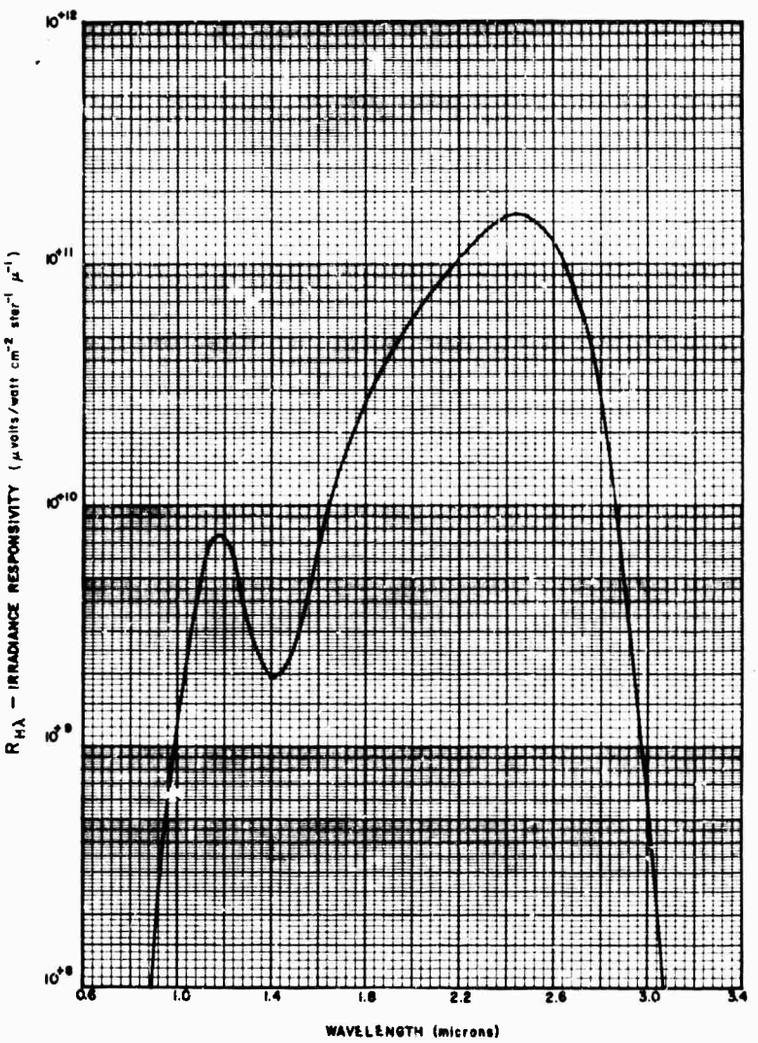

Figure B2. I-14 Irradiance Responsivity (PbS Channel)

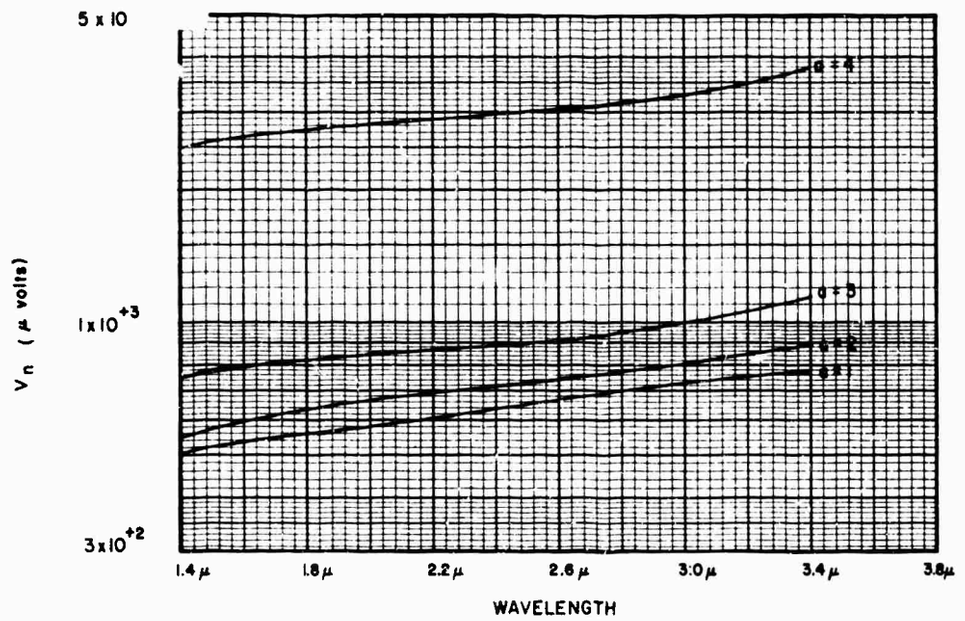

Figure B3. I-14 Electronic Noise Level as a Function of Attenuation State (PbS Channel)

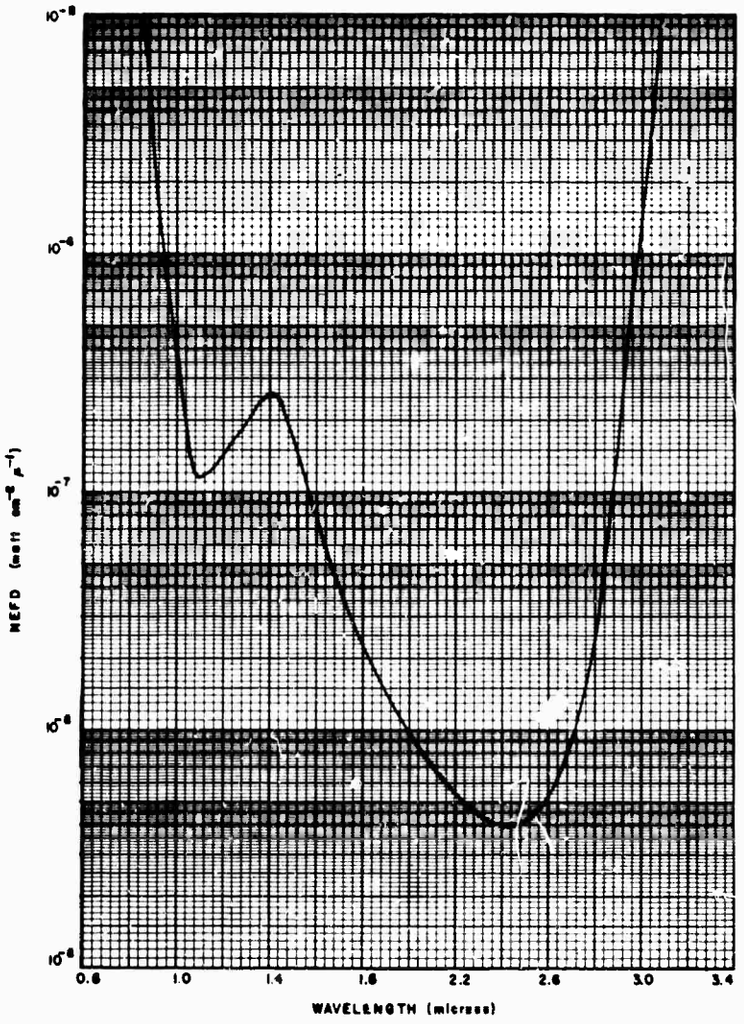

Figure B4. I-14 Noise Equivalent Flux Density (PbS Channel)

of view (Figure B5). Because of the relatively low output frequencies of the bolometer channel, the noise level as a function of attenuation state is slightly greater (Figure B6). For states 3 and 4, V_N is not shown as no laboratory source was strong enough to effect the change. By dividing V_N by the irradiance responsivity, the noise equivalent flux density of the bolometer channel was obtained (Figure B7).

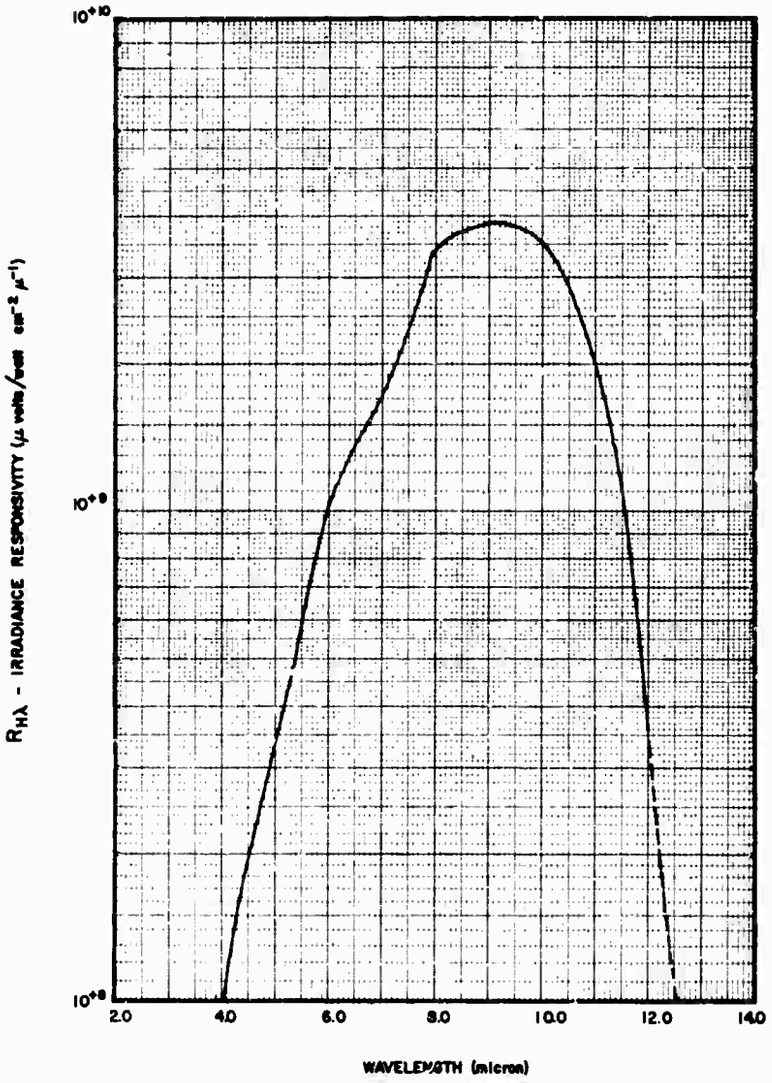

Figure B5. I-14 Irradiance Responsivity (Bolometer Channel)

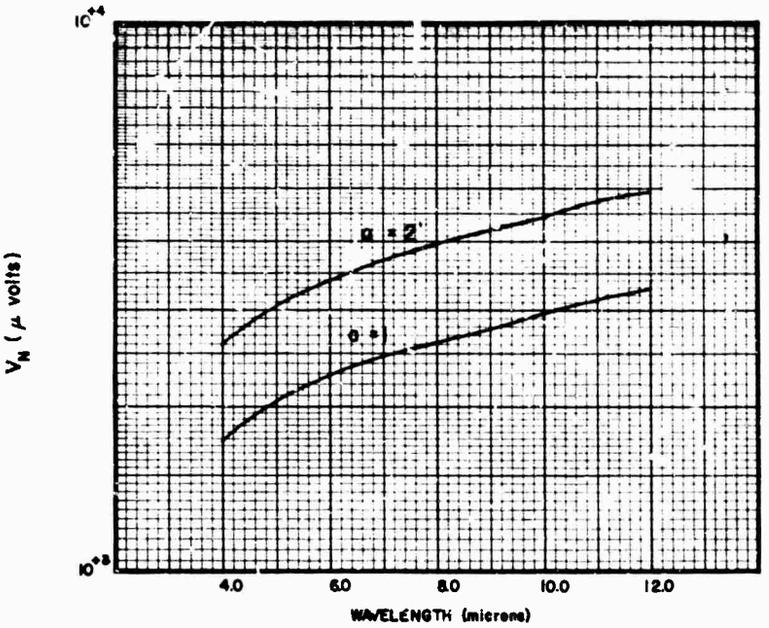

Figure B6. I-14 Electronic Noise Level (Bolometer Channel)

6. FIELD OF VIEW

The field of view curves given in Figures B8 and B9 were measured by irradiating the instrument with collimated radiation and rotating it while the collimator remained fixed; the target subtended an angle of approximately 0.005 radians. Two orthogonal cuts were made for each channel; the solid lines in the figures were made across the longitudinal axis of the instrument. An average of the two cuts was used to compute the solid angle, assuming a conical field of view.

7. RESPONSIVITY VERSUS TEMPERATURE

As in the case of the E3G Radiometer, the PbS channel of the I-14 was sensitive to change in temperature. Calibration of the PbS thermistor (Figure B10) was performed in a temperature chamber while exposing the instrument to a constant source. The increase in responsivity with temperature (Figure B11) is typical for this type of detector; irregularities encountered near room temperatures are due to imperfect compensation of the instrument electronics for thermal changes. The bolometer detector did not show any significant variation consistent with the instrument monitored temperatures.

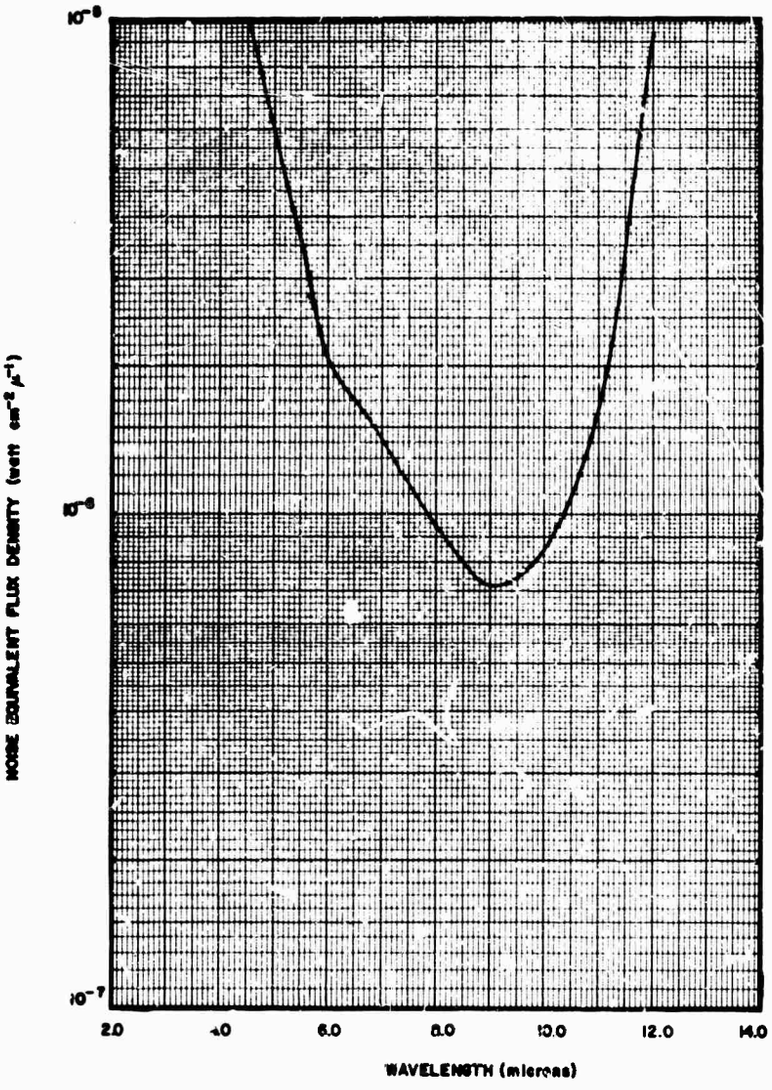

Figure B7. I-14 Noise Equivalent Flux Density (Bolometer Channel)

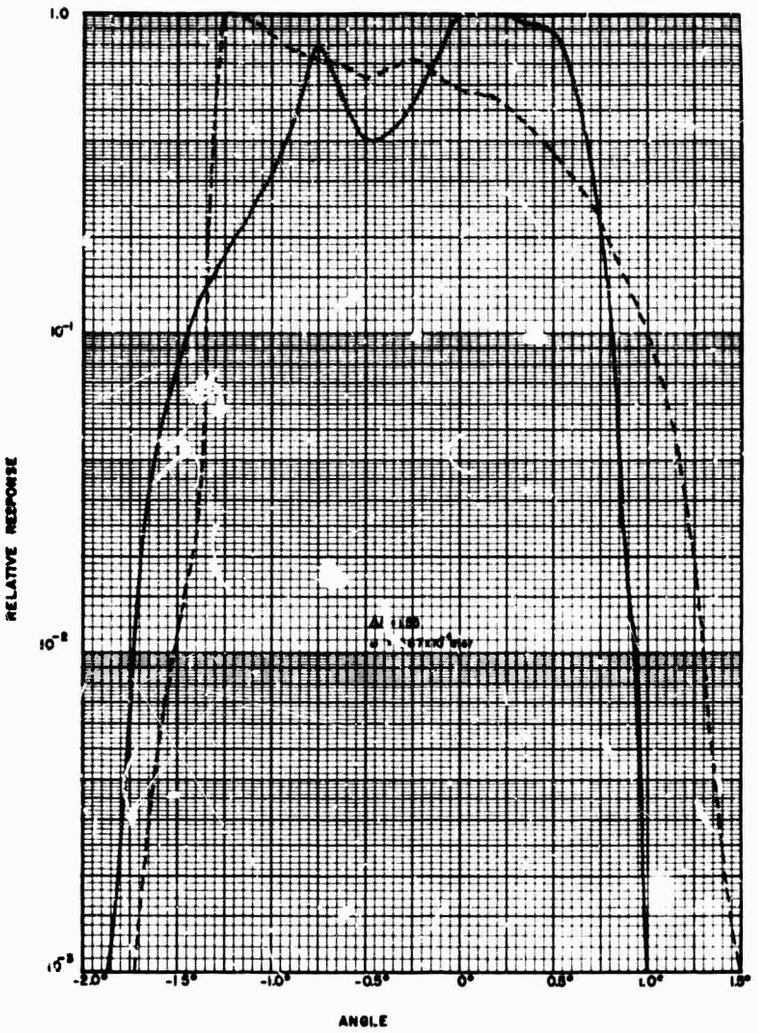

Figure B8. I-14 Interferometer Field of View (PbS Channel)

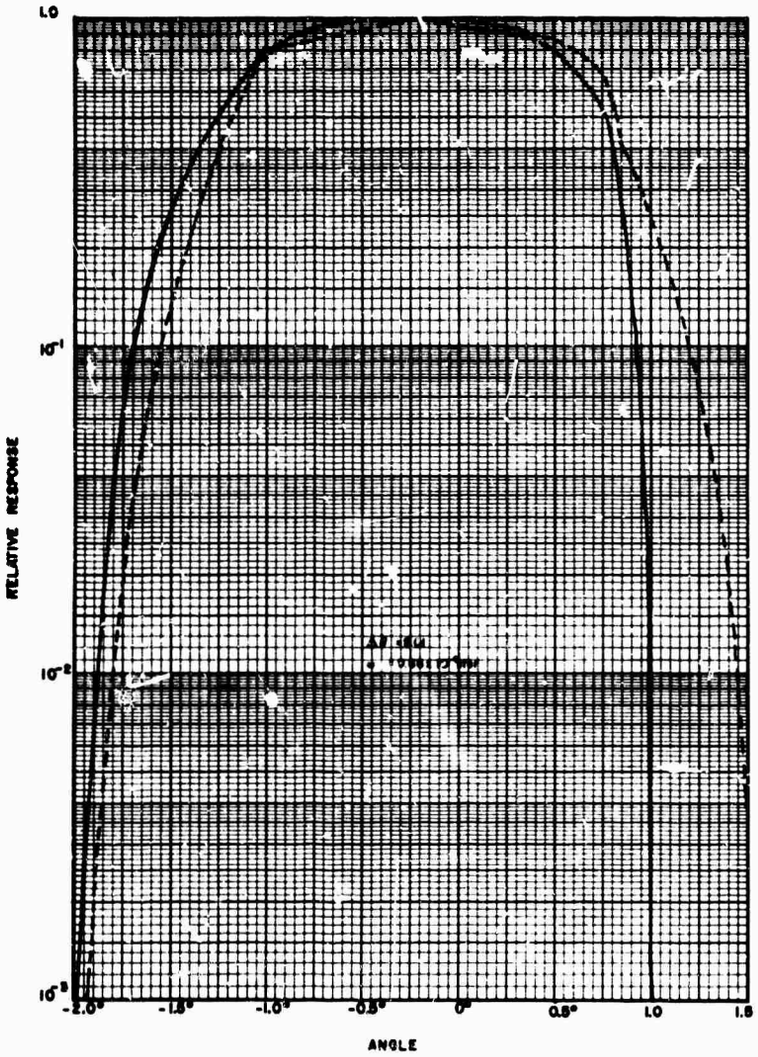

Figure B9. I-14 Field of View (Bolometer Channel)

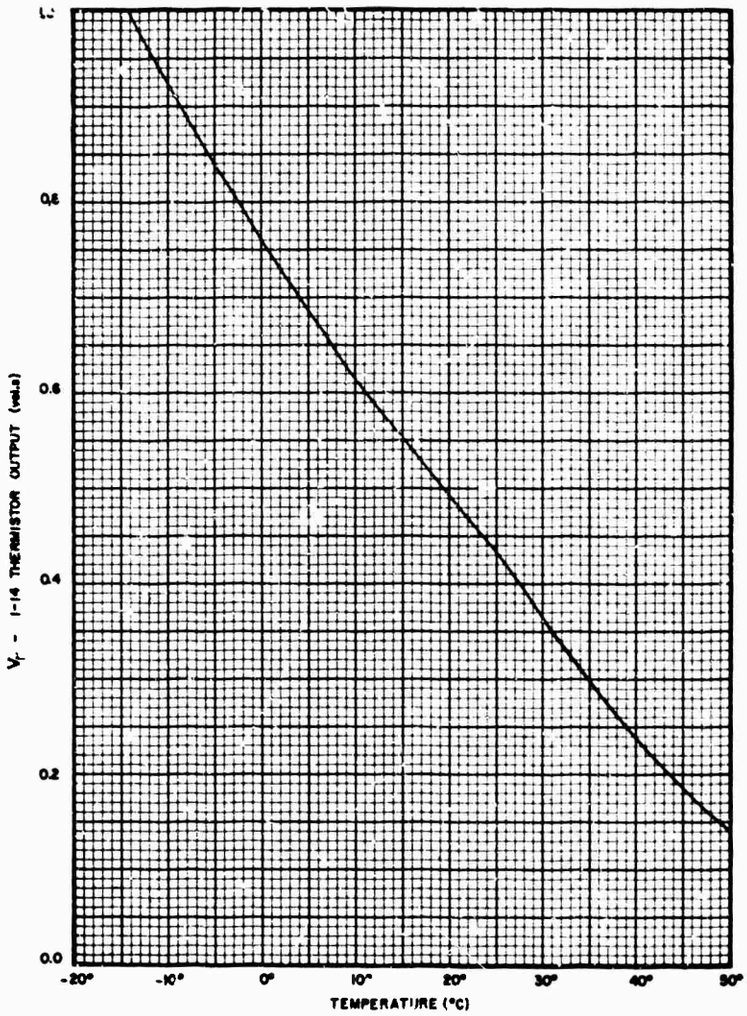

Figure B10. I-14 Thermistor Output as a Function of Temperature (PbS Channel)

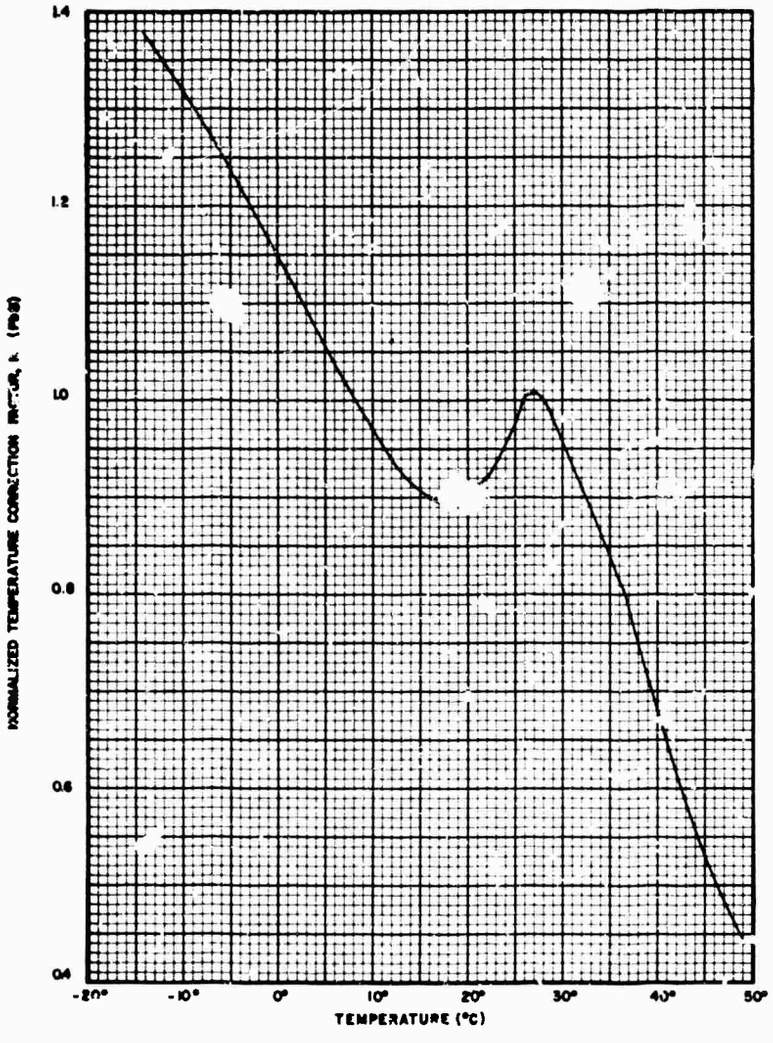

Figure B11. I-14 Normalized Temperature Correction Factor (PbS Channel)

8. THE DICHROIC FILTER PROBLEM

The dichroic filter used to divide the energy between the two detectors in the Gemini V interferometer was a long-wavelength pass-interference filter deposited on a barium fluoride substrate. Long-wavelength pass-interference filters of this type invariably have "bumpy" transmittance characteristics in their pass region; this is also true of very wide bandpass interference filters. A rise in the transmittance of the Gemini V interferometer dichroic filter near 1.4μ caused a dip in the spectrum reflected to the PbS detector (Figure B2). This problem is identical to that described in the Gemini VII interferometer calibration (Condron and Nadile, 1966). In this case, however, the reflection characteristics of the dichroic were poorer from 1.0 to 1.5μ resulting in very poor signal to noise in this region of the spectrum. As a consequence of the spectral imbalance created by the dichroic, relatively strong continuous targets would force the instrument into a higher attenuation state, thereby maintaining the poor response at the short wavelength end of the spectrum. Though this problem was evident during the calibration, scheduling conditions made it impossible to change the filter in time to meet the delivery date for installation on the spacecraft.

9. DATA REDUCTION METHODS

In order to correct the amplitude and frequency of the telemetered data to compensate for inflight changes in instrument response, the I-14 was provided with a filtered calibration lamp mounted in the secondary of the Cassegrain telescope. As there was no provision for occulting incident radiation during calibration light operation, its energy was added to the target intensity over the filter bandwidth.

An analyzed spectrum of the calibration lamp (optics covered) is shown in Figure B12 in terms of the second attenuation state output voltage $\left(V_{2(t+n)}\right)$. This voltage level was used to correct all the data prior to analysis. Since the intensity of the calibration lamp was found to be independent of instrument temperature, this correction superseded the temperature correction factor K shown in Figure B10. Thus, the analyzed PbS spectral output $V_t(\lambda)$ was evaluated by the equation

$$H_\lambda = \frac{V_t(\lambda)}{R_H(\lambda)} \quad (\text{watt cm}^{-2}\,\mu^{-1}) \tag{B6}$$

$$N_\lambda = \frac{V_t(\lambda)}{\omega R_H(\lambda)} \quad (\text{watt cm}^{-2}\,\text{ster}^{-1}\,\mu^{-1}) \tag{B7}$$

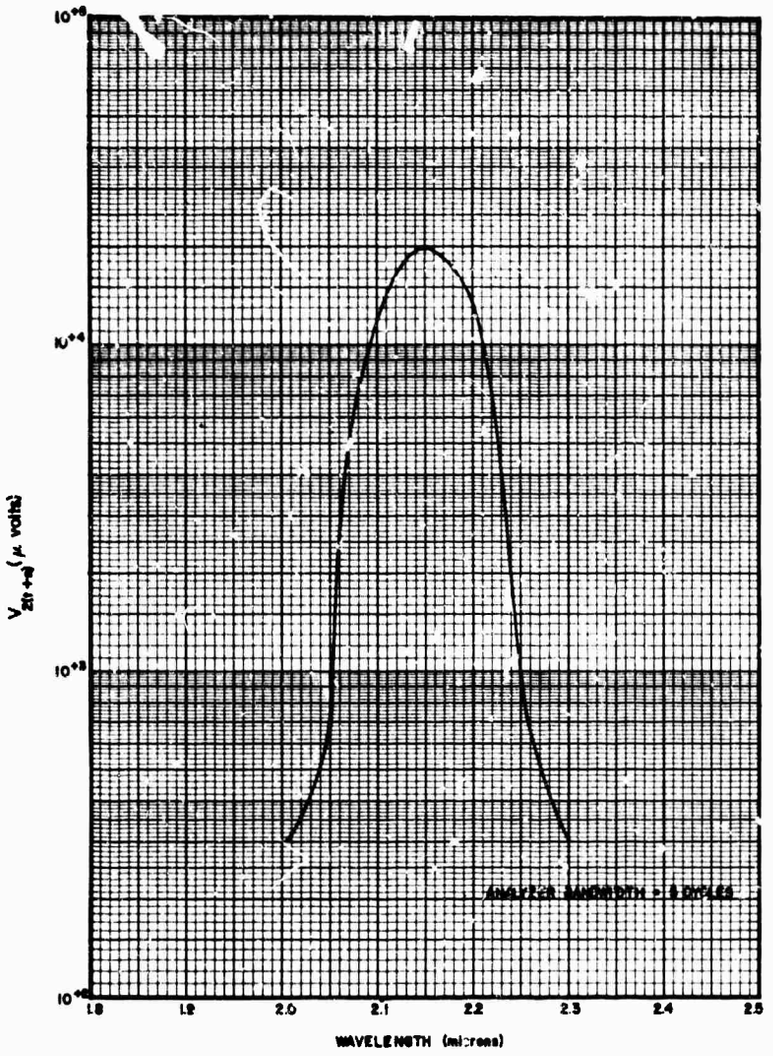

Figure B12. Analyzed Calibration Light Spectrum (Attenuation State 2 - PbS Channel)

where

ω = 5.67×10^{-4} steradians

$R_H(\lambda)$ = responsivity vs λ in Figure B2

V_t = corrected output voltage (Eq. B4).

Similarly, by measuring the frequency of the calibration light filter peak, correction could be made for a change in the value of ν /f. This was done in conjunction with the CO_2 absorption bands observed when looking through the earth's atmosphere; unlike the Gemini VII interferometers, no ν/f correction was necessary.

Due to the marginal sensitivity of the bolometer channel, no data with signal to noise sufficient for analysis were obtained. Although the instrument was primarily designed as a PbS interferometer, the bolometer detector was included in the hope that it would detect targets with colder temperatures than the bolometer detector at little additional cost. Detection of cold targets was not possible because the dichroic filter temperature was too high.

BLANK PAGE

Appendix C

Gemini V Interferometer Calibrations
I-15 Interferometer Serial 003

1. DESCRIPTION

The I-15 interferometer spectrometer was an open cycle, cryogenically cooled interferometer using a mercury-doped germanium detector for operation in the 8 to 13 μ region. A complete description of the instrument and the calibration techniques used have been given in Nadile, Turner, Marcotte, and Lovett (1967). No repetition will be made here.

2. IRRADIANCE CALIBRATION

A near-field calibration using a black body source with a 0.040-in. aperture 5 inches from the primary lens was the only calibration made. Due to condensation resulting from impurities in the liquid neon coolant, only one temperature run at 285°K was successful. The spectral irradiance responsivity and noise equivalent flux density based on this calibration are shown in Figures C1 and C2. Like Serial 001 launched on Gemini VII, a conical field of view of 9.57×10^{-4} steradians was assumed. This resulted in almost identical responsivities at the 12-μ peak.

3. ν /f CALIBRATION

Since only one good calibration spectrum was analyzed, only one value of ν/f was obtained (8.37 cm^{-1}/Hz). However, indications from earlier unsuccessful calibration attempts reveal a ν/f drift similar to that encountered in the Gemini VII interferometer. Hence, it was assumed that the error in absolute responsivity was as great or greater than that of the Gemini VII I-15.

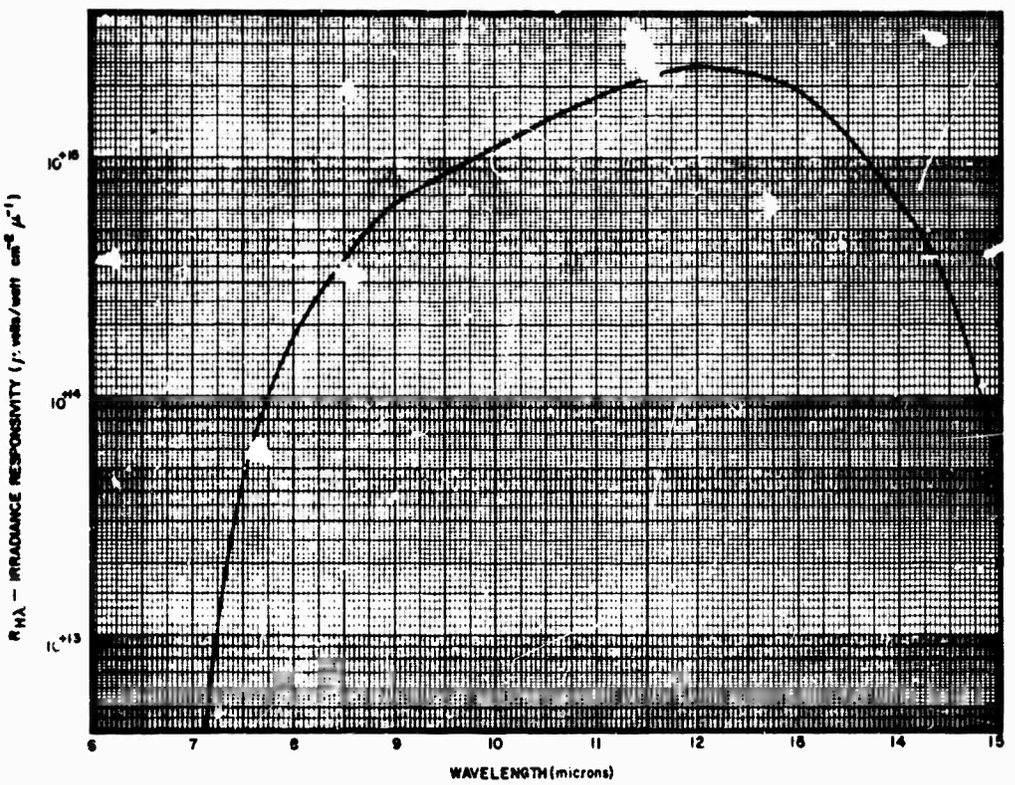

Figure C1. Spectral Irradiance Responsivity of I-15 Cryogenic Spectrometer

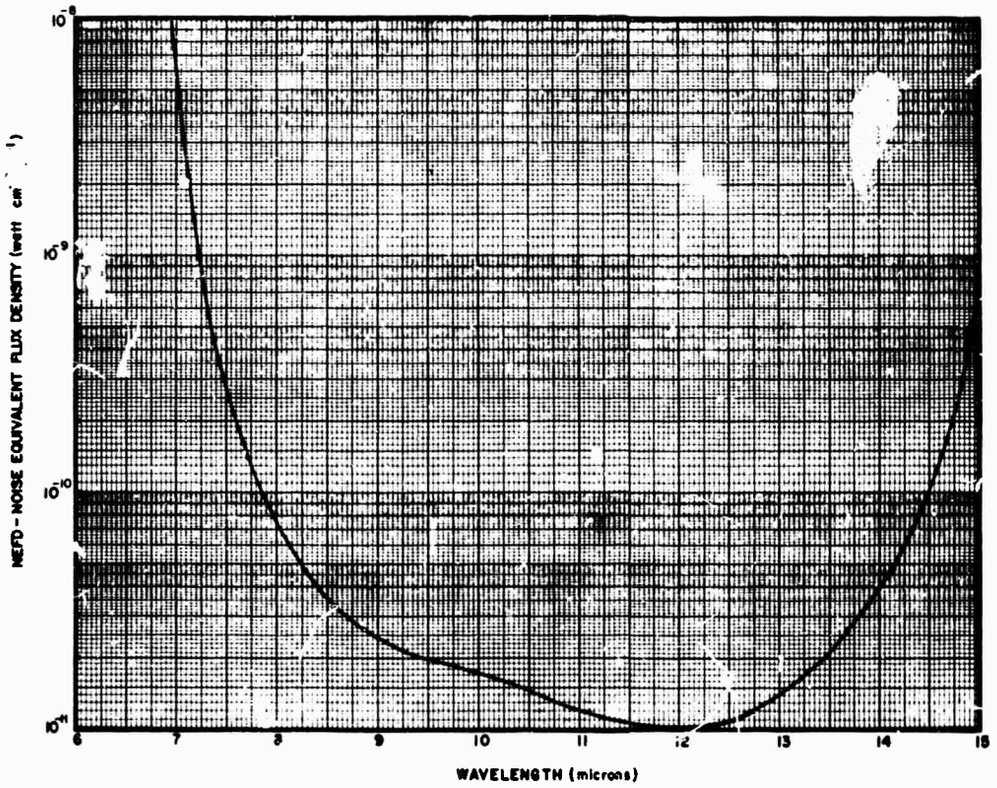

Figure C2. Noise Equivalent Flux Density of I-15 Cryogenic Spectrometer

DOCUMENT CONTROL DATA - R&D

(Security classification of title, body of abstract and indexing annotation must be entered when the overall report is classified)

1. ORIGINATING ACTIVITY *(Corporate author)*
Air Force Cambridge Research Laboratories (CRO)
L. G. Hanscom Field
Bedford, Massachusetts 01730

2a. REPORT SECURITY CLASSIFICATION
Unclassified

2b. GROUP

3. REPORT TITLE
GEMINI V D4/D7 SPECTRAL MEASUREMENTS OF SPACE OBJECTS AND EARTH-CLOUD BACKGROUNDS

4. DESCRIPTIVE NOTES *(Type of report and inclusive dates)*
Scientific. Interim.

5. AUTHOR(S) *(First name, middle initial, last name)*
J. Lovett
L. Marcotte
R. Nadile

6. REPORT DATE
October 1967

7a. TOTAL NO. OF PAGES
69

7b. NO. OF REFS
8

8a. CONTRACT OR GRANT NO.
ARPA Order No. 363

b. PROJECT, TASK, WORK UNIT NOS. 8662-00-01

c. DOD ELEMENT 62503015

d. DOD SUBELEMENT

9a. ORIGINATOR'S REPORT NUMBER(S)
AFCRL-67-0563

9b. OTHER REPORT NO(S) *(Any other numbers that may be assigned this report)*
AFSG No. 198

10. DISTRIBUTION STATEMENT
Distribution of this document is unlimited. It may be released to the Clearinghouse, Department of Commerce, for sale to the general public.

11. SUPPLEMENTARY NOTES
Supported by the Program SSC 631A. Partially supported by ARPA, Order No. 363

12. SPONSORING MILITARY ACTIVITY
Air Force Cambridge Research Laboratories (CRO)
L. G. Hanscom Field
Bedford, Massachusetts 01730

13. ABSTRACT

Results of the radiometric and interferometric optical measurements performed by the crew of Gemini V during the D4/D7 experiment are presented. With use of a rapid-scan Michelson PbS Interferometer and two radiometer channels filtered at 2.2μ and 4000 Å, measurements of earth and lunar reflected sunlight are compared to those obtained on the Gemini VII flight. Also included are detailed calibrations of the D4/D7 instrumentation used on Gemini V.

DD FORM 1 NOV 65 1473

14. KEY WORDS	LINK A		LINK B		LINK C	
	ROLE	WT	ROLE	WT	ROLE	WT
Gemini V Spectral Measurements						